

ScholarWorks@GSU

Chronostratigraphy of Barva and Poas Volcanoes, Volcanic Central Cordillera, Costa Rica

Authors	Guerrier, Anjelica
Citation	Guerrier, Anjelica. Chronostratigraphy of Barva and Poas Volcanoes, Volcanic Central Cordillera, Costa Rica. Aug. 2018, Georgia State University. https://doi.org/10.57709/12559987 .
DOI	https://doi.org/10.57709/12559987
Download date	2026-03-09 21:07:39
Link to Item	https://hdl.handle.net/20.500.14694/6318

CHRONOSTRATIGRAPHY OF BARVA AND POAS VOLCANOES, VOLCANIC
CENTRAL CORDILLERA, COSTA RICA

by

ANJELICA GUERRIER

Under the Direction of Paulo Hidalgo

ABSTRACT

The chronostratigraphy from >50,000 BP to the present was determined for the overlapping tephra deposits from Barva and Poas volcanoes, located 20 km north of San Jose, Costa Rica, using stratigraphic correlations supported by fourteen C¹⁴ ages. The 16 km proximity of the cones, the abundance of vegetation that overlays the tephra facies, high rates of weathering and erosion, and presence of cinder cones make unraveling the eruptive history of the two volcanoes problematic. Previous attempts have been made to develop an eruptive history of the tephra deposits between the Barva and Poás volcanoes, but relied on stratigraphic correlations based only on physical characteristics of tephtras. Developing an accurate eruptive history is crucial for the assessment of volcanic risk, which could prove imperative to surrounding communities that could be significantly affected by caving roofs, disrupted agriculture and water supply, and respiratory ailments.

INDEX WORDS: Chronostratigraphy, Fall deposits, Eruptive history, Poás, Barva, Cordillera
Central, Tephra

CHRONOSTRATIGRAPHY OF BARVA AND POAS VOLCANOES, VOLCANIC
CENTRAL CORDILLERA, COSTA RICA

by

ANJELICA GUERRIER

A Thesis Submitted in Partial Fulfillment of the Requirements for the Degree of

Master of Science

in the College of Arts and Sciences

Georgia State University

2018

Copyright by
Anjelica Ashley Guerrier
2018

CHRONOSTRATIGRAPHY OF BARVA AND POAS VOLCANOES, VOLCANIC
CENTRAL CORDILLERA, COSTA RICA

by

ANJELICA GUERRIER

Committee Chair: Paulo Hidalgo-Odio

Committee: Hassan Babaie

Brian Meyer

Electronic Version Approved:

Office of Graduate Studies

College of Arts and Sciences

Georgia State University

August 2018

DEDICATION

This thesis is dedicated to my parents, Sandy and Brian Hoggard, whose love and support have carried through my academic career.

ACKNOWLEDGEMENTS

First, I would like to thank Dr. Paulo Hidalgo whose guidance has been imperative to my development as a geologist. I would like to thank Dr. Brian Meyer and Dr. Hassan Babaie for serving as members of my thesis committee. I would also like to thank the students of the Costa Rican Study Abroad of 2016 and 2017 for helping with data collection.

TABLE OF CONTENTS

ACKNOWLEDGEMENTS	V
LIST OF TABLES	IX
LIST OF FIGURES	X
1 INTRODUCTION	12
1.1 Significance.....	12
1.2 Previous Works	12
1.3 Objectives.....	14
1.4 Study area	14
1.4.1 Site description	14
1.5 Tectonic setting.....	16
1.6 Background	17
1.6.1 Volcanic deposits.....	17
1.6.2 Fall deposits.....	18
2 METHODS	19
2.1 Collection process.....	20
2.2 Column correlations	20
2.3 Radiocarbon dating	21
3 RESULTS	22
3.1 Field Observations	23

3.2	Example Column.....	24
4	DISCUSSION.....	26
4.1	Depositional Environments(NAME OF SECTION)	26
4.1.1	<i>Cinder cones</i>	26
4.1.2	<i>Lahars</i>	28
4.1.3	Similar Units	31
4.1.4	<i>Sedimentation rates</i>	31
4.1.5	<i>Weathering and erosion</i>	31
4.1.6	Erosional surfaces and unconformities	32
4.2	Correlations.....	35
4.3	Periods of activity	35
4.3.1	PB Sequence 1	35
4.3.2	<i>Sabana Redonda</i>	41
4.3.3	<i>PB Sequence 2</i>	44
4.3.4	<i>PB Sequence 3</i>	47
4.3.5	<i>PB Sequence 4</i>	52
4.4	Further Implications.....	55
4.4.1	<i>Northern Sector</i>	0
4.4.2	<i>Southern Sector</i>	0
4.4.3	<i>Western Sector</i>	2

4.4.4	<i>Eastern Flank</i>	3
4.5	Spatial Relationships	4
4.6	Interpretations	4
4.6.1	<i>Barva</i>	4
4.6.2	Poás	5
5	CONCLUSIONS	5
6	RECOMMENDATIONS	9
	REFERENCES	10
	APPENDICES	13

LIST OF TABLES

Table 1: Sample Log. The table depicted above contains all of the dated samples collected in this study. All of the dates were determined using carbon-14 analysis. Sample Po-2a resulted in a date that was greater than 50,000 years BP, which lies outside of the accuracy of the calibration software, and thus was left uncalibrated. The colors of the dates correlate to those of the columns.

..... 22

LIST OF FIGURES

Figure 1 Stratigraphic Column Locations	16
Figure 2 tectonic map.....	17
Figure 3 Plinian Eruption Controls.....	19
<i>Figure 4. PB Sequence 4 correlation.....</i>	Error! Bookmark not defined.
Figure 5. PB Sequence 1 (layers A-C).....	Error! Bookmark not defined.
Figure 6. PB Sequence 1 (layers D-F)	Error! Bookmark not defined.
Figure 7 PB Sequence 1 (layer E).....	Error! Bookmark not defined.
Figure 8 PB Sequence 1 (layers J-L)	Error! Bookmark not defined.
Figure 9. SabanaRedonda Unit	Error! Bookmark not defined.
<i>Figure 10. Sabana Redonda Cross Section</i>	Error! Bookmark not defined.
Figure 11. SabanaRedonda Outcrop	Error! Bookmark not defined.
Figure 12 .PB Sequece 2 Correlation.....	Error! Bookmark not defined.
Figure 13. PB Sequence 3 Correlation.....	Error! Bookmark not defined.
Figure 14 PB sequence 3 (layers E and F).....	Error! Bookmark not defined.
Figure 15 Claibration curves of PB Sequence 3	Error! Bookmark not defined.
Figure 16 PB Sequence 3 outcrop modern eruptions.....	Error! Bookmark not defined.
Figure 17 PB Sequence 4 Correlation A.....	Error! Bookmark not defined.
Figure 18. PB Sequence 4 Correlations B	Error! Bookmark not defined.
Figure 19. North-South Sector A	57
Figure 20. North-South Sector B	59
Figure 21. East-West Sector A.....	61
Figure 22. East-West Sector B.....	63

Figure 23. Diagnostic of PB Sequence 3 3

Figure 24 Composite Column..... 8

1 INTRODUCTION

1.1 Significance

The region encompassing both the Barva and Poás volcanoes, just north of San Jose, Costa Rica, is one that has developed agricultural roots in coffee and sugarcane, as well as the cultivation of livestock. The recent activity experienced at the Poás volcanic center within the last year has raised concerns about the safety of this popular tourist destination. Natural hazards, like volcanic eruptions, are uncontrollable and can pose a threat to the people of surrounding communities. Although the threat of eruptions cannot be removed, they can be managed by studying past events to create hazard maps, which allow for proper evacuation and mitigation planning, and predictions of future events. The only way to ensure accurate predictions is to start with accurate hazard maps that illustrate the possible magnitude and intensity of future eruptions. Previous attempts at generating hazard maps of this location have used less reliable methods for producing the maps. This study seeks to improve upon those methods for the production of more accurate hazard maps for the communities that occupy this region.

1.2 Previous Works

There have been previous studies conducted in this area in the past that have produced hazard maps, but they have proven to be fairly unreliable. Past studies have provided information about the study area, but have been more geochemically and/or petrologically focused, such as the study conducted by Kussmaul & Sprechmann (1982).

Prosser & Carr (1987) conducted research that defined the changing chemical composition of three magmatic series on the top sector of Poás Volcano, while Brenes (2003) used geochemical techniques to identify the layers that compose the Barva

Formation. Studies of the tephra layers associated with the individual craters of the two volcanoes were comprehensive, but the chemistry was associated with particular layers that were correlated on the basis of physical characteristics alone. Without the certainty brought on by multiple radiometric dates, the correlations, and thus the geochemistry associated with each layer, cannot be verified. Correlations between tephra stratigraphic units becomes more difficult when extrapolating the physical and geochemical components associated with the volcanic centers, to that of overlapping tephra deposits that lie between Barva and Poás.

In addition to the difficulties associated with interlayered deposits, there are a series of tephra cones located south of the Poás crater that further disrupt the original deposition of the tephra (Gazel & Ruiz, 2005). As a result, there are various types of deposits found in and around the Barva and Poás volcanoes that require investigation beyond the physical characteristics of the tephra layers. One study, performed by students at the University of Costa Rica (Peraldo et al., 2003), attempted to characterize the eruption style of Barva. Isopach maps were created and it was stated that Barva was distinguishable by its strombolian eruptions. All of the conclusions were based on one C^{14} date. Identifying correlations amongst multiple stratigraphic columns without multiple dated samples allows for substantial amounts of error. Fall deposits are complex and can vary in thickness and grain-size overtime, factors on the basis of which the correlations of that study were made, and can be reworked by wind or water, making correlations more difficult without more supporting evidence (Rosi, 2015).

The overlapping tephra layers in this area create a complex setting of overlapping volcanic deposits that cannot simply be explained by physical similarities

amongst tephrastatigraphic layers. In order to ensure more accurate correlations between tephra layers, additional geologic analysis, incorporating numerous radiometric ages, needed to be made to construct a complete chronostratigraphic representation of the study area.

1.3 Objectives

The purpose of this study is to construct a complete eruptive history of the volcanic deposits that lie between the Poás and Barva craters. The production of effective hazard maps is contingent upon the accuracy of this eruptive reconstruction. The work that was carried out to meet this goal is as follows:

- 1) Record data from facies of volcanic deposits that can be used to create tephrastatigraphic columns.
- 2) Identify correlations within the tephrastatigraphy of various columns and confirm those correlations through the use of carbon-14 dating or chronostratigraphic
- 3) Develop a comprehensible compilation of the stratigraphic columns in the form of one composite chronostratigraphic representation of all observed tephra layers.

This study aims to create a more accurate eruptive history of Barva and Poás to make way for more effective hazard maps to be produced in the future, which could ultimately save thousands of lives in the surrounding communities.

1.4 Study area

1.4.1 Site description

The study area is located in the highlands of the Cordillera Central, approximately twenty-five kilometers north of San Jose, Costa Rica, and encompasses the area between

two volcanoes, Poás and Barva. There is a relatively small distance between the two craters, about 15 kilometers, that ultimately resulted in overlapping tephra deposits. Due to its location in such a tropical environment, much of the ground cover is highly vegetated, and many of the volcanic deposits are intensely weathered. This fact creates a more difficult environment for data collection.

In an effort to preserve this volcanically active region of Costa Rica, several national parks were established. The areas that surround the parks are now occupied with private landowners and business to support the tourist economy. Although some of the establishments made desired column locations inaccessible, the expansion of roads created an advantage, as some of the largest exposures of underlying strata were found along road cuts. Columns were constructed for the area between the western slope of Barva and the eastern slope of Poás (see Figure1).

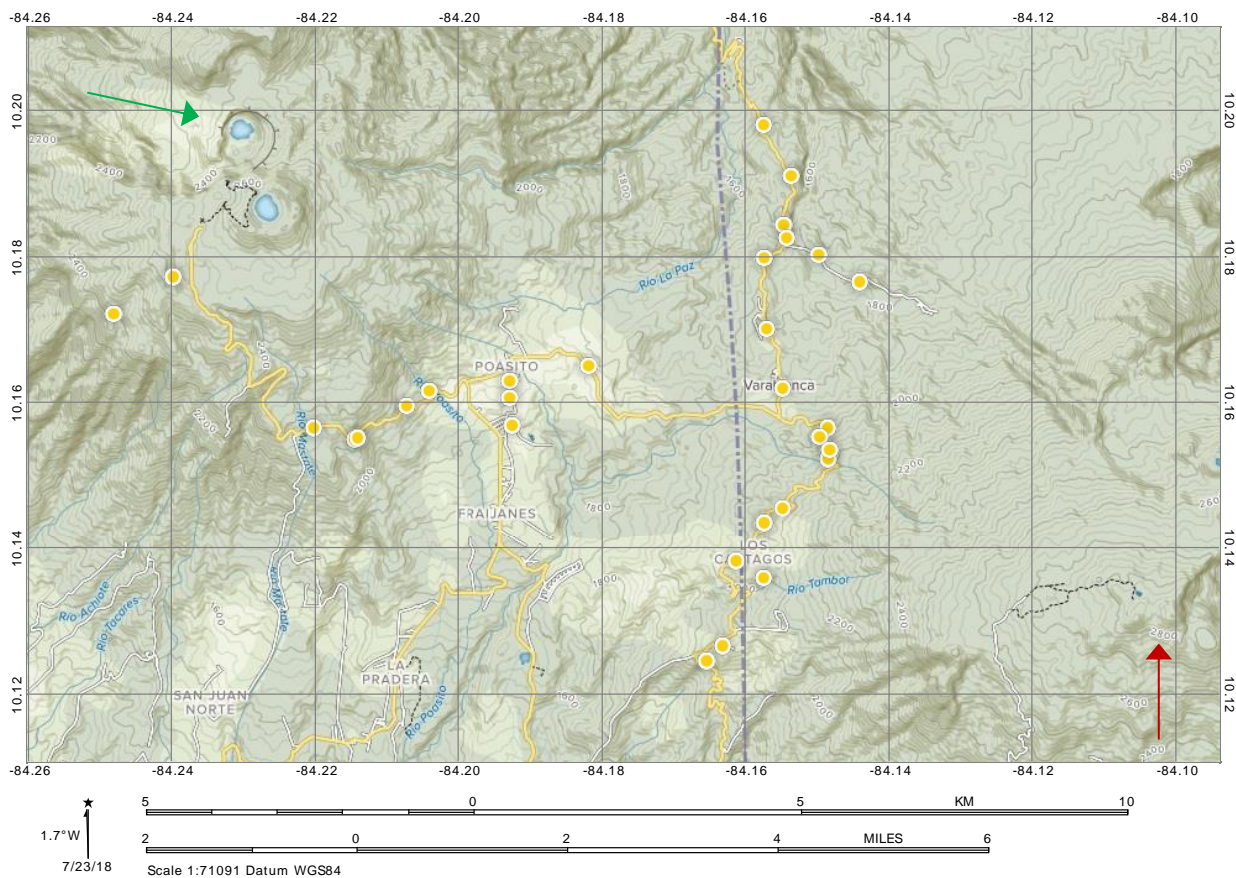


Figure 1: Stratigraphic Column Locations. The stratigraphic columns collected in this study are labelled on the map. The Poás crater is depicted in the northwest corner of the map, indicated by the green arrow. The Barva crater lies in the southeastern corner of the map, indicated by the red arrow, but is less prominent than that of Poás.

1.5 Tectonic setting

The Cordillera Central is among the many volcanic formations that comprise the Central America Volcanic Arc that runs roughly parallel to the Central American coastline. This mountain range has a length of about 80 kilometers, and reaches a maximum elevation of 3,432 meters. There are five main volcanic centers located within the cordillera: Porvenir, Poás, Barva, Irazú, and Turrialba. The volcanism associated with this area is attributed to the subduction of the Cocos Plate beneath the Caribbean Plate,

estimated at a rate of about 10mm per year (Demets, 2001). This conglomeration of volcanic massifs formed as a result of the retreating volcanic arc of Costa Rica. The volcanic front within the Cordillera Central marks the migration of the magmatic edifice that once occupied the area below the Cordillera de Aguacate (Marshall, 2003). The advancement of the Costa Rican volcanic arc is due to evolution of the subduction angle by which the downgoing Cocos plate slips.

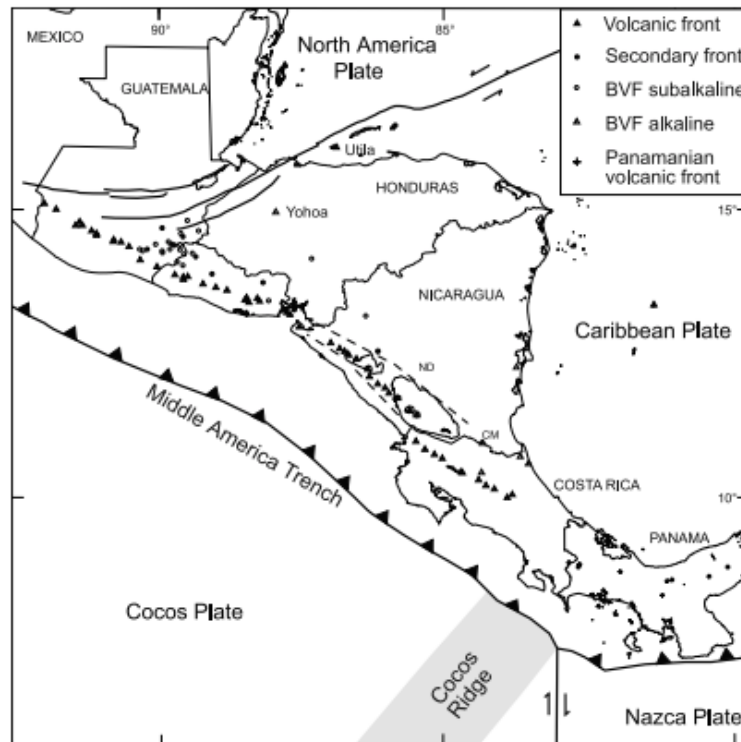


Figure 2: Tectonic map. Map illustrating the tectonic plates (Cocos Plate Subducting below the Caribbean) (Carr and Alvarado, 2007).

1.6 Background

1.6.1 Volcanic deposits

During a volcanic eruption, various types of material are ejected and deposited in the areas surrounding the crater. All airborne material is referred to as tephra that can be broken down into subcategories based on grain-size. Grain-size fragments less than or

equal to two millimeters are considered ash, fragments two to sixty-four millimeters are lapilli, and anything greater than sixty-four millimeters is labeled as a bomb. The fragments can be composed of pumice, lithics, or scoria, a vesicular fragment that often has a mafic composition. When these are settled and compacted, sometimes welded, into a layer they are known as volcanic tuff.

1.6.2 Fall deposits

Many of the deposits within the study area are characterized by pyroclastic deposits (Brenes, 2003), many of which have been labeled as plinian or subplinian events. These types of tephra deposits are recognizable by their tendency to evenly blanket topography and thin outward from the volcanic focus. There are many parameters that affect the way in which these deposits are distributed such as fragmentation, wind field, and differing plume characteristics (Cioni and Rosi, 2015). Figure 3 illustrates some of the considerations in effect during pyroclastic eruptions and how plume height controls the dispersal of pyroclastic deposits (Pyle, 2015). By combining known information about the dispersal and fragmentation of a particular pulse or event, the type and intensity of an eruption can be determined using a formula proposed by Walker (1973). Given the number of variables that can affect deposition of fall deposits, it becomes more difficult to correlate volcanic tuffs. This fact highlights the need for a study with extensive radiocarbon dating to determine the eruptive history.

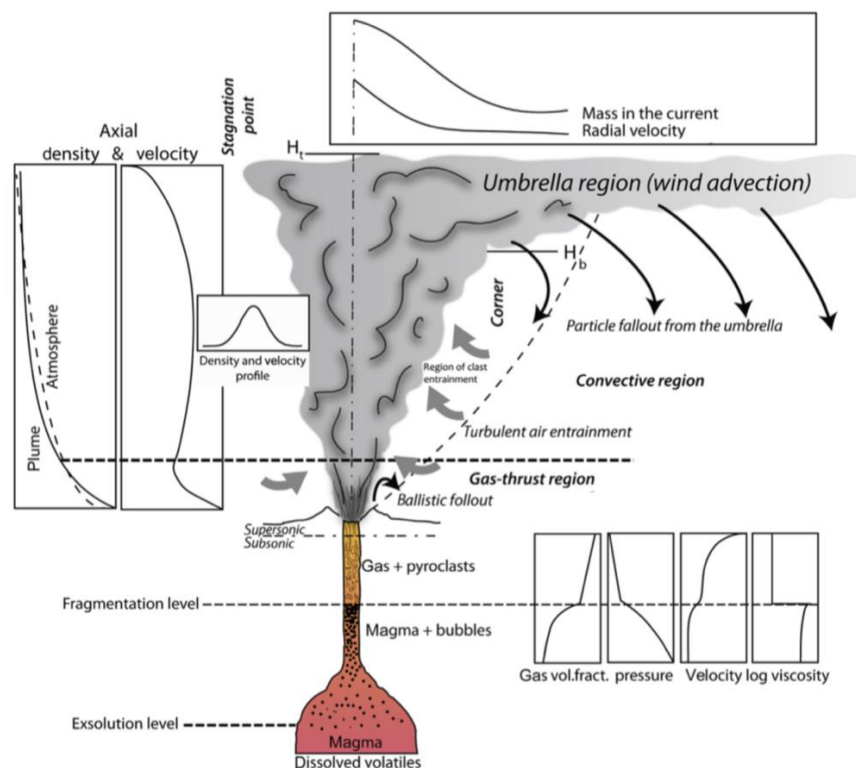


Figure 3: Plinian Eruption Controls. Illustration of the general parameters that control plinian eruptions. (Rosi, 2015).

2 METHODS

This research was conducted in the highlands of the Cordillera Central, an area located in the Alajuela Province. Forty-two stratigraphic columns were extracted for locations that fall between the Barva and Poás volcanoes. Two main sets of stratigraphic columns were produced, one running north to south, and the other running east to west. The column locations were selected to reflect the orientation of the preferential wind direction, which flows southwest (Campaña Geológica, 2004). Tephra deposits are controlled by wind and result in depositional patterns reflecting the trend of the paleo wind direction (Cioni & Pistolesi, 2015). The column locations were also selected based on the quality of an outcrop, where columns were spaced at least fifty meters apart to encompass the entire study area; inaccessibility due to businesses and

private landowners limited some of the desired locations. A majority of the columns were made along road cuts, as these contain some of the most substantial exposures of underlying strata.

2.1 Collection process

To create the stratigraphic columns, tephra faces were exposed by removing any vegetation that had accumulated on the surface. Machetes were used to remove thick vegetation, and weed scrapers were used to produce a fresh exposure of the underlying tephra layers, allowing for more accurate observations. The grain sizes, sorting, level of oxidation, and percentage of pumice and lithics were recorded. The true thickness of the stratigraphic layers, which were distinguishable by variances in their physical characteristics, were also recorded. Samples of organics, such as paleosols and charcoal, were taken when they were present within the tephra layers at the column locations; later to be dated using C^{14} . The samples were carefully extracted, so as not to contaminate it with carbon and oils from human hands, and stored in aluminum foil to ensure preservation.

2.2 Column correlations

In an effort to determine the extent of each eruptive event, comparisons between the columns were made. Some of the tephra layers exhibited unique characteristics that allowed them to be discernable amongst the other tephra stratigraphic layers. These layers were deemed as marker beds and helped in revealing the relationships that existed amongst the columns. Other studies have used a similar correlation method, but the accuracy of the correlations is questionable, as there were no radiometric ages applied to justify their correlations. This study has incorporated fourteen C^{14} ages, allowing for more accurate correlations to be made. The lack of dated material in previous studies has led to less reliable correlations, and thus interpretations of the geochronology of the volcanic strata are subject to error.

2.3 Radiocarbon dating

The samples were submitted for radiocarbon analyses to the Center for Applied Isotope Studies (CAIS) at the University of Georgia (UGA). The samples went through a physical pretreatment process in which they were manually sorted and sieved. In samples for which the plant material was dated the Acid/Alkali/Acid (AAA) method was used as an acid pretreatment to the sample. The AAA method is a three-step process in which (1) an initial acid treatment is applied to remove any secondary carbonates; (2) humic acids are then eradicated with an alkali treatment, and lastly (3) a secondary acid treatment is performed to eliminate any atmospheric CO₂. For the organic samples in which the substrate was purely soil and sediment, hot HCl was used as an acid pretreatment to remove any acid-soluble compounds. The samples were then put in 1M HCl and kept at 80 °C for one hour; afterward, the samples were centrifuged and decanted. The samples were then rinsed with DI water and dried at 60 °C. Dated plant material requires a few extra steps: a 0.1 M NaOH solution, used to eliminate any contamination of humic acid, and a dilute HCl treatment was performed before being rinsed and dried. The pretreated samples were then placed in evacuated quartz ampoules that contain CuO and were then combusted at 900 °C to yield CO₂. The CO₂ was then purified cryogenically so that it could be condensed in traps located on a vacuum line, which uses liquid nitrogen. The purified CO₂ gas was then converted to graphitic carbon by reducing the CO₂ that is exposed to hydrogen at 580 °C, all within a closed system exposed to iron. The iron serves as a heat conductor, binder, and catalyst. The sample was then ready to be run in an Accelerated Mass Spectrometer (AMS). The laboratory ages were calibrated, using the CALIB Version 7.1.html software (Stuiver; Reimer, 2018).

3 RESULTS

Through observation and data collection, forty-two columns were created to illustrate the tephra-stratigraphic sequence throughout the study area. Of these columns, twenty-three were selected for making correlations. The columns excluded from correlation were ones that were either in close proximity (within 40m) to another column and thus combined into one, did not extend to a reasonable depth beneath the subsurface, or were decidedly too oxidized to decipher between tephra layers. The samples taken within the stratigraphic columns were primarily composed of organic-rich soils, but a few consisted of charcoal or preserved wood. Several samples were collected, and fifteen of those samples were dated using C¹⁴, resulting in ages ranging from 1,870 (± 134) BP to 50,850 (± 580) BP, found in *Table 1*.

The samples were collected at different times in the duration of this research, over the course of two years. Stratigraphic correlations were refined multiple times as more samples were sent for dating, again, highlighting the importance of incorporating several radiometric dates. The ages allowed for more difficult correlations, those containing multiple units with similar physical characteristics or that have been heavily affected by weathering in which units are unrecognizable, between columns to be made. The columns, in which samples were collected, are accompanied by their calibration curves and are illustrated in the appendix.

Table 1: Sample Log.

The table contains all of the dated samples collected in this study. All of the dates were determined using C¹⁴ analysis. Sample Po-2a resulted in a date that was greater than 50,000 years BP, which lies outside of the accuracy of the calibration software, and thus was left uncalibrated. The colors of the dates correlate to those of the columns.

Column ID	Sample ID	Material Type	Laboratory Ages	Calibrated Age (BP)	Long	Lat
AK-0	Po-121517_1	soil	13,290 +/- 40	15,982 +/- 92	-84.157	10.180
AK-0	ARK 1-4	soil	12,720 +/- 40	15,160 +/- 70	-84.157	10.180
AK-1	AK 2-1	soil	20,200 +/- 55	24,269 +/- 107	-84.220	10.156
AK-3	AK 3-1	soil	2,230 +/- 25	2,225 +/- 34	-84.214	10.155
AK-4	Ak 4-1	soil	18,319 +/-57	22,202 +/-57	-84.207	10.159
AK-13	VB 2	soil	22,320 +/- 55	24,615 +/-143	-84.149	10.152
AK-19	JJ 2-2	wood	200 +/- 20	172 +/-12	-84.165	10.124
AK-22	Ak-22 B	soil	28,460 +/- 80	32,442 +/- 248	-84.158	10.144
AK-24	Po-4	charcoal	5,300 +/- 25	4,134 +/- 20	-84.193	10.157
AK-24	Po_509_A	soil	9,910 +/- 30	11,292 +/- 34	-84.193	10.157
AK-24	Po_509_C	soil	21,720 +/- 50	25,962 +/-66	-84.193	10.157
AK-25	Po-121517_2	soil	17,370 +/- 45	20,954 +/- 98	-84.162	10.139
AK-26	Po_13	soil	2,830 +/- 25	2,931 +/- 22	-84.233	10.167
AK-26	Po_14	soil	4,530 +/- 25	5,153 +/- 68	-84.233	10.167
AK-27	Po_0510_1D	soil	7,120 +/- 25	7,953 +/-17	-84.248	10.173
AK-29	Po_509_2	soil	14,220 +/- 35	17,456 +/- 77	-84.193	10.163
AK-31	Po-2a	charcoal	50,850 +/- 580	N/A (>50k)	-84.214	10.155

3.1 Field Observations

Field observations yielded a variety of different tephra deposits including a range of grain sizes and distributions, different degrees of weathering and oxidation, and variances in pumice and lithic concentrations, all of which can be used to determine the style of eruption. These observations were used to distinguish between tephra layers, known as volcanic tuff, to create stratigraphic columns. Pyroclastic material is classified according to grain size, where ash is defined by particles <2mm, particle ranging between 2 and 64mm are considered lapilli, and bombs are anything greater than 64mm. The physical attributes of each tuff were placed into categories of deposits, in which the

primary classifications were based on resistance and grain size. The tephra layers were categorized in the following ways:

- a) Lava flow: only one was located and was characterized by a dark aphanitic texture
- b) Agglomerate: deposit containing welded scoria bombs
- c) Ash tuff: this term is redundant, as a tuff is defined as a tephra layer composed of ash sized particle, but is used to highlight the distinction between lapilli tuffs.
- d) Hard ash tuff: the tuff contains ash sized particles with a relatively high resistance to weathering (often difficult to scrape).
- e) Lapilli tuff: tephra composed mainly of lapilli fragments that has medium to low resistance
- f) Hard lapilli tuff: tephra similar to that in a lapilli tuff but has a higher resistance to weathering (often difficult to scrape)
- g) Ash soil: type of transitional soil that has experienced weathering and with a low ash to matrix ratio
- h) Lapilli soil: type of transitional soil that has experienced weathering with a low lapilli to matrix ratio
- i) Soil: topsoils and paleosols fall into this category and are abundant in organic material

3.2 Example Column

Observations made in the field were converted to digital illustrations, created in Adobe Illustrator, using the tephra descriptions listed above (letters a-i), as seen in Figure 4. The visual format of each column made patterns in the stratigraphy more apparent, thus simplifying the initial correlation process. Some of the patterns observed in the tephra stratigraphy include

discernable units that appear in the same sequential order between columns (see discussion), and their thickness throughout the study area.

AK - 1



Figure 4: Visual conversion of field observations. The column, AK-1, was created in Adobe Illustrator by applying the deposit delineation described in (3.1) to observations described in the field. The numbers attached to the strata to the left of column coincide with the descriptions on the right. This process was repeated for all forty-two columns.

4 DISCUSSION

The depositional environment in the study area is one marked by several explosive volcanic events, indicated by the abundance of pyroclastic fall deposits from at least two main volcanic edifices. In an area where lava flows are far and few between, especially in the more recent stratigraphy visible near the main crater of Poás (Prosser & Carr, 1987), radiometric dating is a necessary tool for identifying the stratigraphic relationships amongst tephra layers. Characteristics of the tephra deposits in the area provide evidence of massive eruptions, erosional contacts, cinder cones, lahars, and landslides. These features coupled with overlapping deposits from adjacent volcanic centers has created a complex research setting, in which deciphering between separate volcanic pulses is challenging.

4.1 Depositional Environments

The highlands of the Cordillera Central are inundated with pyroclastic deposits of varying grain sizes, thicknesses and pumice concentrations resulting from plinian, subplinian, strombolian, and phreatomagmatic style eruptions (Cioni and Pistolesi, 2015). The physical attributes of tephra layers in the study area also indicate discontinuity in deposition, resulting in unconformities and several erosional surfaces. The types of deposits observed in the area explain some of the causes of these unconformities.

4.1.1 *Cinder cones*

Cinder cones are typically asymmetric, conical shapes shaped by wind direction. The cones are primarily composed of scoria ejected from explosive activity, often strombolian eruptions, with a dry magma source that is basaltic to andesitic in composition. The deposits are red in color due to oxidation from hot gasses at the central part of the volcanic edifice. The outer crust/walls of these cones are commonly black or gray due to lack of oxidation (de Silva and

Linsay, 2015). The agglutinate deposit found in column AK-23 (Figure 5) adheres to this definition, where the welded scoria deposits displayed a dark gray color, suggesting observation of the outer portion of the cone. These deposits were also described by Gazel and Ruiz (1987), and identified as series of cinder cones, known as Sabana Redonda (Figure 5), oriented along fissure networks found in the southern flank of Poás. These deposits differ from the surrounding tephra deposits and contribute to the difficulty of correlating fall deposits in the area. A charcoal deposit was found within a tephra layer that underlays the agglomerate unit of Sabana Redonda and was dated at 50,850 BP, supporting the finding in Campañas Geologica (2004).

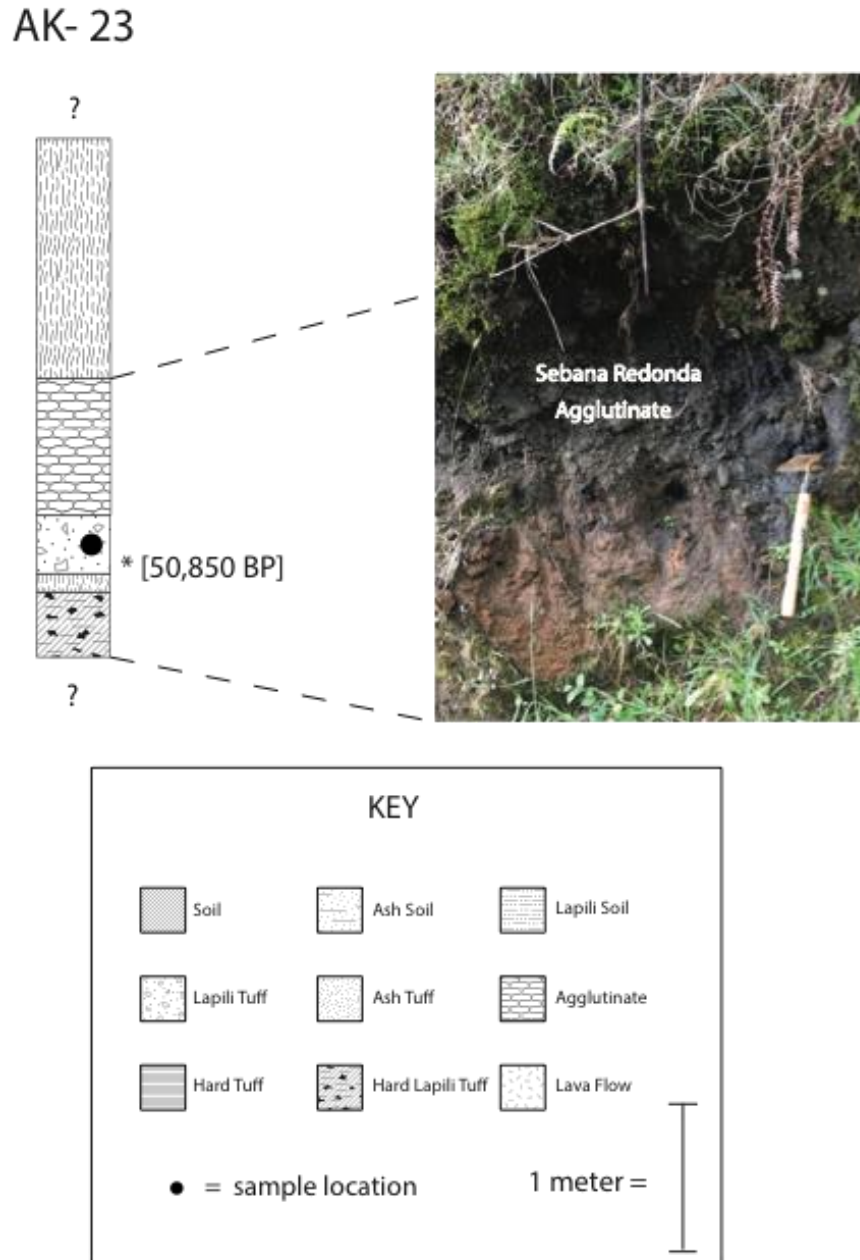


Figure 5: Sabana Redonda Unit Exposure in Column AK-23. The photo to the right captures the physical exposure of the agglutinate deposit of the Sabana Redonda Unit.

4.1.2 Lahars

These rapidly flowing, water-saturated mixtures of rock, debris, and water are unconsolidated and extremely poorly sorted. These flows need an adequate water supply,

abundance of unconsolidated debris, like that found in a pyroclastic or fall deposits, and steep slopes. Lahars and debris flows can often times be triggered by flank collapses, especially if deposits are weakened by hydrothermal activity or oxidation and leaching of tropical soils, like those found in Costa Rica. This flow typically creates a large erosional surface, especially when steep slopes are underlain by less resistant deposits. Lahars often times scour out and incise river channels that infill with lahar deposits of unconsolidated, poorly sorted material, especially as flows become more water-saturated. The deposits found in column AK-27 (Figure 6) contain these same characteristics and are illustrated in figure 5. This layer is assumed to be the result of a lahar, possibly linked to the crater collapse associated with the main crater, mentioned by Prosser and Carr (1987).

AK - 27

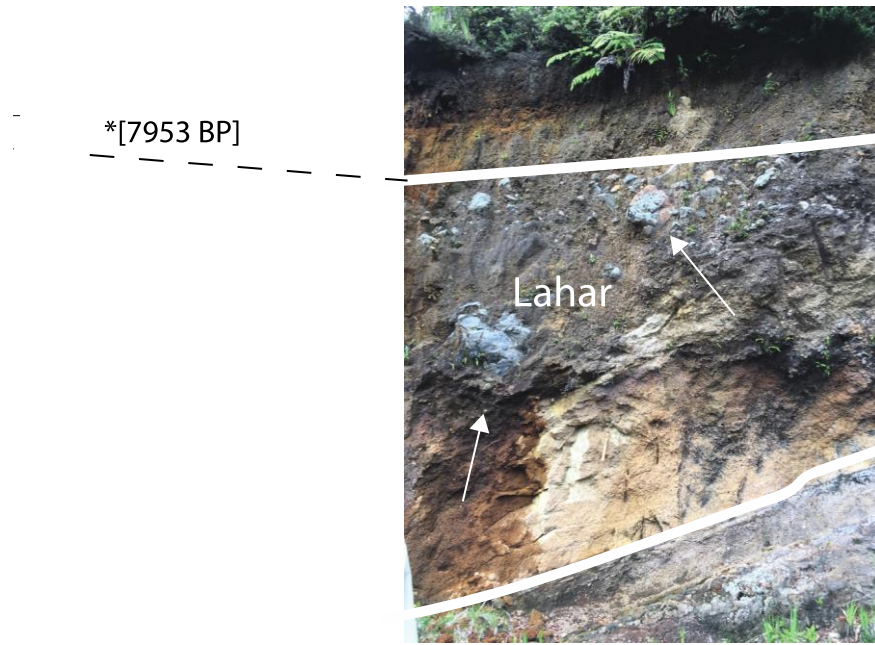


Figure 6: Lahar Deposit in AK-27. The image to the right illustrates the incising nature of lahar deposits. The deposition from the lahar is unsorted and contains large blocks, indicated by the white arrows.

4.1.3 *Sedimentation rates*

Sedimentation rates are primarily controlled by the frequency and continuity of deposition, which for pyroclastic flows, is usually sporadic and unsteady. The fragmented characteristic of many pyroclasts result in strata with fairly low preservation potentials; usually eroded completely within several hundreds of thousands of years, depending on the thickness of the sedimentation and length of hiatuses (Deligne & Sigurdsson, 2015). The abundance of pyroclastic deposits in the study area, coupled with their naturally low preservation potential can account for thickness variations and sometimes lack of exposure of tephra layers in some of the stratigraphic columns .

4.1.4 *Weathering and erosion*

Another obstacle that increases the complexity of the deposits in the Alajuela Province is the high rate of erosion and weathering, as a result Costa Rica's tropical climate. The higher rates of erosion in the area are attributed to greater amounts of oxidation caused by exposure to moisture and oxygen, often leading to secondary erosional features such as landslides. These mass wasting events further disrupt the stratigraphic sequence and compound the effects of low sedimentation rates by creating additional unconformities and discontinuities in tephra layers. (see figure 6). Oxidation continues to act on these deposits at greater rates as surface area increases with each event. Aside from landslides, heavy oxidation can degrade tephra facies, resulting in less distinguishable physical characteristics, making correlations on these characteristics alone subordinate to those backed by radiometric dating (see figure 7).



Figure 7: Heavily Weathered Tuff. The photo above is an example of a highly oxidized ash tuff. This deposit still slightly resembled an ash, as few grains were able to be distinguished. Although this tephra was able to be identified as an ash, some deposits are too oxidized to be identified.

4.1.5 Erosional surfaces and unconformities

Pyroclastic fall deposits are often times easily eroded and can result in many gaps in the volcanic record of the area (Pyle, 2015), one example being lahars, as seen in figure 5.

Pyroclastic events can also create strong surges that create high energy surfaces along which predated pyroclastic flows can be eroded. Periods of little deposition and/or those associated with a hiatus are more affected by erosion. Erosional surfaces can cause lateral pinching due to uneven surfaces in the topography, resulting in variable thicknesses; increasing the difficulty of identifying and correlating tephra layers. Another example can be seen in column AK-0, where

many of the tephra layers seen in adjacent columns are not present. The discontinuation of of these tephra layers can be explained by the erosional contact indicated in red in figure 8.

AK-0

34

Figure 7: Erosional Surface Found in Column AK-0. The dashed red line in the image in the top right represents an irregular surface that has encountered erosion. Eroional surfaces such as this one indicate that portions of the volcanic record have been eroded.

4.2 Correlations

The stratigraphic columns created from field observations were placed adjacent to one another based on aerial distribution. The stratigraphic columns were used to produce a string of correlations running from east to west over the distance of about eleven kilometers, and another covering the distance of about eight kilometers, running north to south. Connections between columns were identified by comparing similar characteristics in the digitalized columns, illustrated in figure 4, and within field observations of tephra layers. C¹⁴ samples were used as a tool for confirming or adjusting correlations to increase their reliability.

4.3 Periods of volcanic activity

During the correlation process, C¹⁴ ages yielded four distinct periods of volcanic activity. The periods of activity, referred to in this study as PB (Poás-Barva) Sequence 1, 2, 3 and 4, permitted for simplified comparisons to be made between sequences of tephtras. This method minimized correlation errors by eliminating complications due to variability of tephra layers throughout the study area. Categorizing the tephtras into periods of activity also created an advantage with locations with scarcities in organic material and missing units. Tephra layers of a particular sequence, with distinctive characteristics, could be identified and compared to other columns to be relatively dated. The PB Sequences are designated by color; detailed description of the layers found in each sequence are provided in the in the following sections.

4.3.1 PB Sequence 1

This sequence includes all lithology types found in outcrops in the study area that lie beneath a charcoal-rich lapilli tuff layer found in column AK-23, with a dated carbon-14 age of

50,850 BP (Figure 9). PB Sequence 1 is composed of large lapilli tuff layers that range in color from a brown to an orange-red in areas with higher oxidation. AK-0 column is located in a road cut that provides a 19m exposure and contains the most complete tephra-stratigraphy of this tephra sequence, and thus is used for describing the strata that make up PB Sequence 1 in Figure 4.

W

AK - 23
 Lat: 10.14381
 Long: -84.1578

AK - 23 E

Lat: 10.180
 Long: -84.157

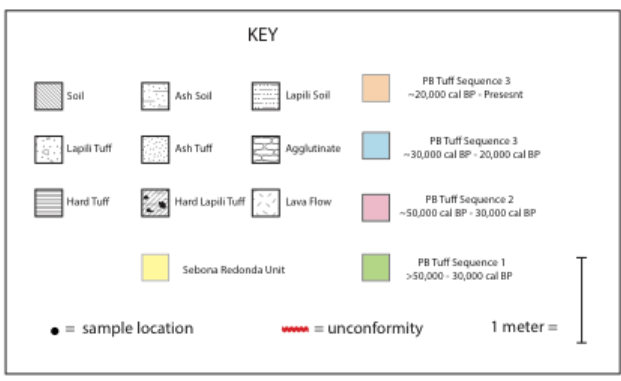
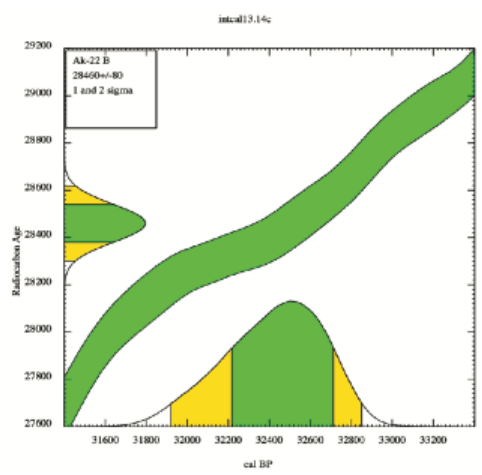
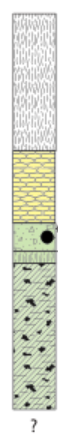


Figure 8: PB Sequence 4 correlation. The above correlation illustrates the location of column AK-0 in relation to column AK-23, as well as the stratigraphic position of PB Sequence 4 in reference to the overlying Sabana Redonta Unit. The calibration curve is also included for the sample in column AK-0. There is no calibration curve for column AK-23 due to the limitations of the calibration software, which is unable to calibrate ages older than 50,000 BP. .

Description of the PB 4 Sequence

- A. This is the lowest layer in the sequence (Figure 10). Fine-grained lapilli to course-grained ash tuff with a concentration of about 10% ≤ 2 mm pumice fragments located towards the top of the tephra layer. This layer outcrops for 40cm in the exposed section, but continues to an unknown depth beneath the subsurface. Contact with the unit above is erosional.
- B. Thin layer of fine-grained gray ash that is exposed as a 10-13cm thick layer in column AK-0. This layer is consolidated and very resistant to weathering. The layer is dark gray in color but contains a thin white layer located at the bottom of the strata as depicted in Figure 10. Contact with the unit above is erosional.

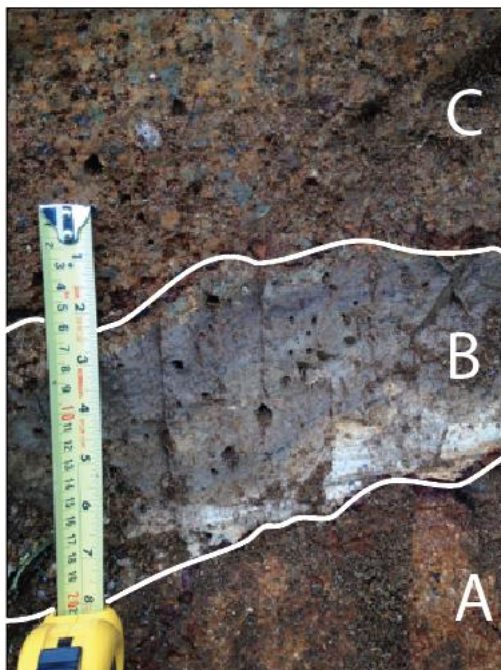


Figure 9: PB Sequence 1 (Layers A-C). The picture above provides visual representation of layers A, B and C of PB Sequence 1.

- C. Lapilli tuff layer is 90cm thick and contains ≤ 1 cm lapilli fragments that are bluish-gray in color. The pumice and lithics appear to have normal grading with a slight fining upward trend.
- D. The strata is a 30cm thick brown lapilli tuff that contains ≤ 1 cm lapilli. (Figure 11)
- E. The gray ash tuff found in this layer is bound by thin, red oxidation layers on both the top and the bottom. The ash bed is 15 cm thick. (Figure 11)



Figure 10: PB Sequence 1 (layers D-F). Layers D, E, and F coincide with those in Figure (4), where D is a fine-grained lapilli tuff, E is a gray ash layer and F is an ashy soil.

- F. A 30cm thick ashy soil serves as a barrier that separates the gray ash tuff in layer E and the overlying hard lapilli tuff in layer G. (Figure 11).
- G. Although this layer consists of a hard lapilli tuff, the media is unconsolidated, as the layer has a crumbly texture that is easily broken apart, illustrated in Figure 12. The

layer is dark and about 3m thick with lapilli grain sizes ≤ 1.5 cm. Lithics are ≤ 5 mm but are found at low concentrations throughout the tephra.



Figure 11: PB Sequence 1 (layer G). An image of layer E of PB Sequence 1

- H. The layer consists of a hard ash tuff that is brown in color and is 20cm thick.
- I. The layer consists of a gray ash tuff with pumice sizes ≤ 1 cm and no presence of lithics.
- J. This is a fine-grained lapilli to course-grained ash tuff that contains ≤ 2 mm pumice grains and lithics of ≤ 4 mm.
- K. The layer is composed of a light gray, fine-grained ash tuff shown in Figure 13. The layer is about 60cm thick and contains a thin layer of oxidation about 17cm from the bottom of the tephra.



Figure 12: PB Sequence 1 (layers J-L). Image of layers J, K, and L of PB Sequence 1. These layers coincide with those shown in Figure 9.

- L. The brown lapilli tuff found in this layer is the thickest lapilli tuff found in the study area and measures to be about 9m thick. The tephra contains lapilli $\leq 1.5\text{cm}$ and lithics of up to 7cm (Figure 13). The tephra has intermittent layers of oxidation throughout. A thin layer of soil separates this layer from the overlying lapilli tuff.

4.3.2 *Sabana Redonda*

This unit is unique from many of the deposits found in the study area, as the source is unrelated to Barva or Poas volcanoes. This deposit originates from a series of five pyroclastic cones that lie on the southern flank of Poás, near a town called Sabana Redonda, and are oriented north-south. The alignment of these cones mimic the fracture network along which the Poás craters are also aligned (Casertano et al., 1983) and is shown in Figure 14.

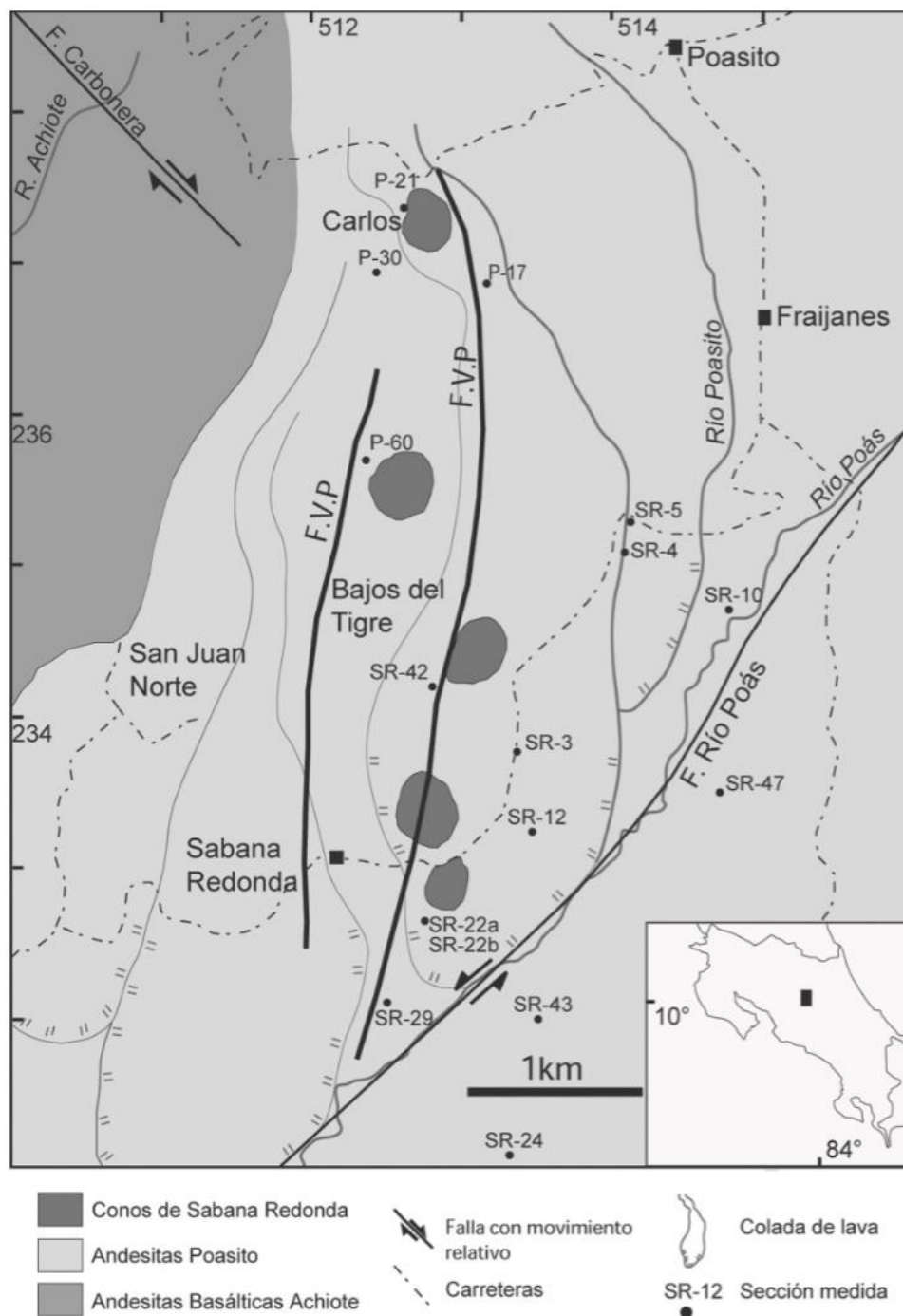


Figure 13: SabanaRedonda Unit. The geologic map around the Sabana Redonda pyroclastic cones. The fracture network is indicated above. Map taken from (Gazel & Ruiz., 2005). Volcan Poas is outside the area of this map.

The Sabana Redonda unit is characterized by scoria bombs and blocks incorporated into a lapilli matrix, identified as agglomerates and aphyric agglutinated lavas. The agglutinate is

composed of welded bombs that average about 33cm in diameter, whereas the flanks can be characterized by thin, fine-medium grained red lapilli (Gazel & Ruiz, 2006). The color of this unit varies from a dark gray to a highly oxidized red color. Gray is associated with paleoenvironments that were dry and did not support high levels of oxidation (Fisher & Schminke, 1984). The different deposits of Sabana Redonda are outlined in Figure 15.

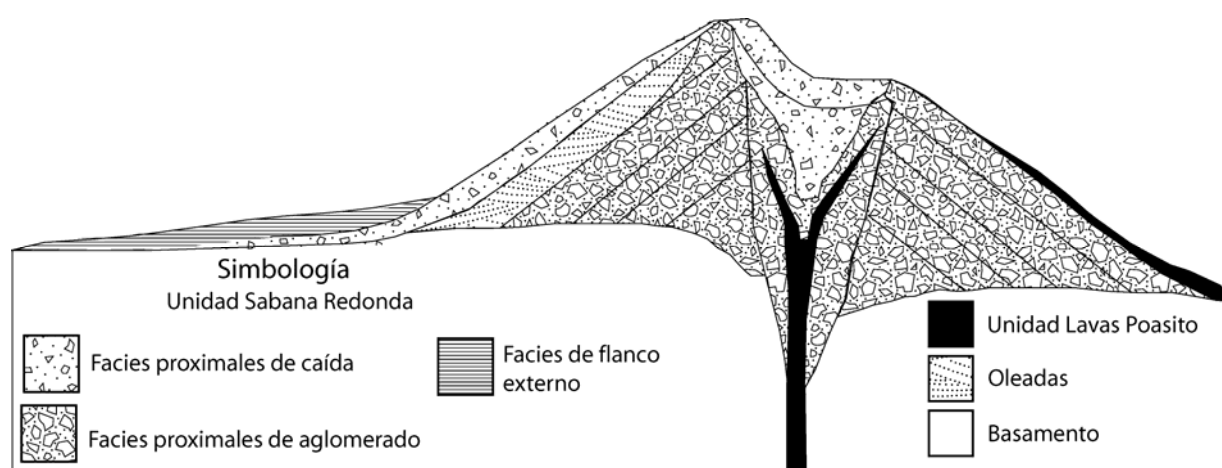


Figure 14: Sabana Redonda Cross Section. The pyroclastic facies of the Sabana Redonda Unit (Vespermann & Schmincke, 2000).

The fall deposits produced by Sabana Redonda have been interpreted as being the product of waves of phreatic events during periods of strombolian activity (Gazel & Ruiz, 2006). A sample was collected between two layers of this unit in column AK-23 (Figure 12) and dated at 50,850 BP. This places the period of activity of this unit after PB Sequence 1 and before PB Sequence 2, as illustrated in column AK-3 (Figure 9).



Figure 15: Sabana Redonda Outcrop. The Sabana Redonda unit composed of agglutinate is illustrated in the image above. The sample taken from column AK-23, dated at 50,850 BP was taken in the location above, as depicted by the arrow.

4.3.3 *PB Sequence 2*

This tephra sequence dates between about 50,000 BP and about 30,000 BP, usually found between PB Sequence 1 and PB Sequence 2, but chronostratigraphically lies above the Sabana Redonda unit.

Description of the PB Sequence 2

- A. Brown ashy soil with ash fragments $\leq 1\text{mm}$ totaling about five percent of the tuff. The ashy soil layer is sometimes seen as a fine lapilli tuff layer north of column AK-0. The bottom of this sequence is bound by the charcoal-rich lapilli tuff found at the top of PB Sequence 1.
- B. The hard ash tuff is a light gray color and contains white silica deposits that resemble roots. The tephra layer caps the top of PB Sequence 2 and is dated at 32,440 cal BP.

The hard ash tuff is missing in some of the columns, such as in columns AK-6, AK-12, and AK-9 (Figure 17), but is always underlain by a transitional soil, identified as an ashy soil in the columns. This layer can be found as thick as half of a meter in column AK-22 (Figure 12).

W

E

AK - 23
 Lat: 10.14381
 Long: -84.1578

AK - 22
 Lat: 10.143
 Long: -84.157

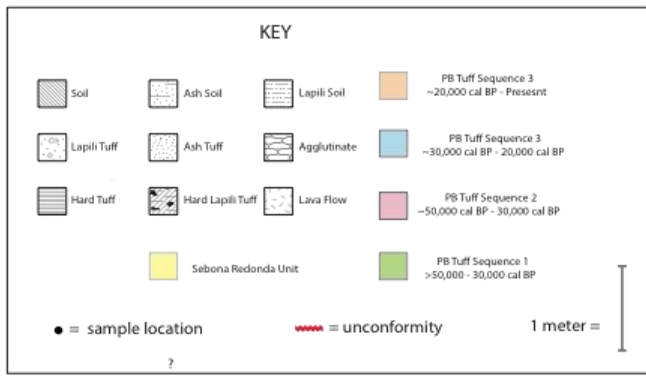
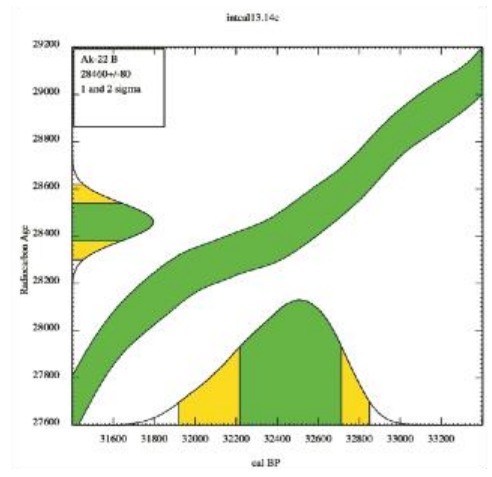
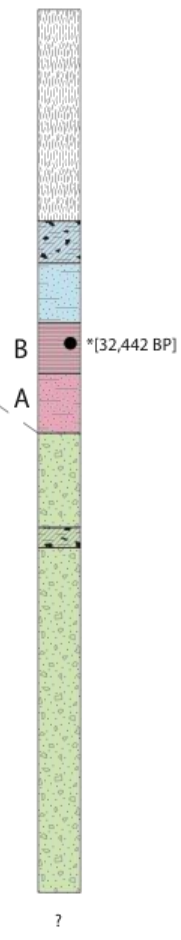
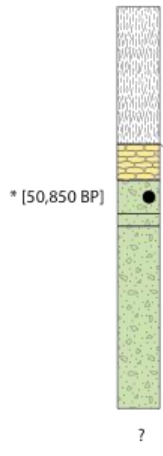


Figure 16: PB Sequence 2 Correlation. The above correlation illustrates the location of column AK-0 in relation to column AK-23, as well as the stratigraphic position of PB Sequence 2 in reference to the overlying Sabana Redonta Unit. The Calibration curve is also included for the sample in column AK-0. There is no calibration curve for column AK-23 due to the limitations of the calibration software.

4.3.4 PB Sequence 3

A compiled sequence of tuffs roughly ranging from about 30,000 cal BP to about 20,000 cal BP serve as the basis of several of the correlations, multiple samples were dated in this range and the tephra layers are very recognizable. Thick sections of this sequence are often exposed in road cuts and this facilitated in the correlation of many of the columns. The summarized stratigraphy of this unit is presented along with detailed descriptions in the following pages.

W

E

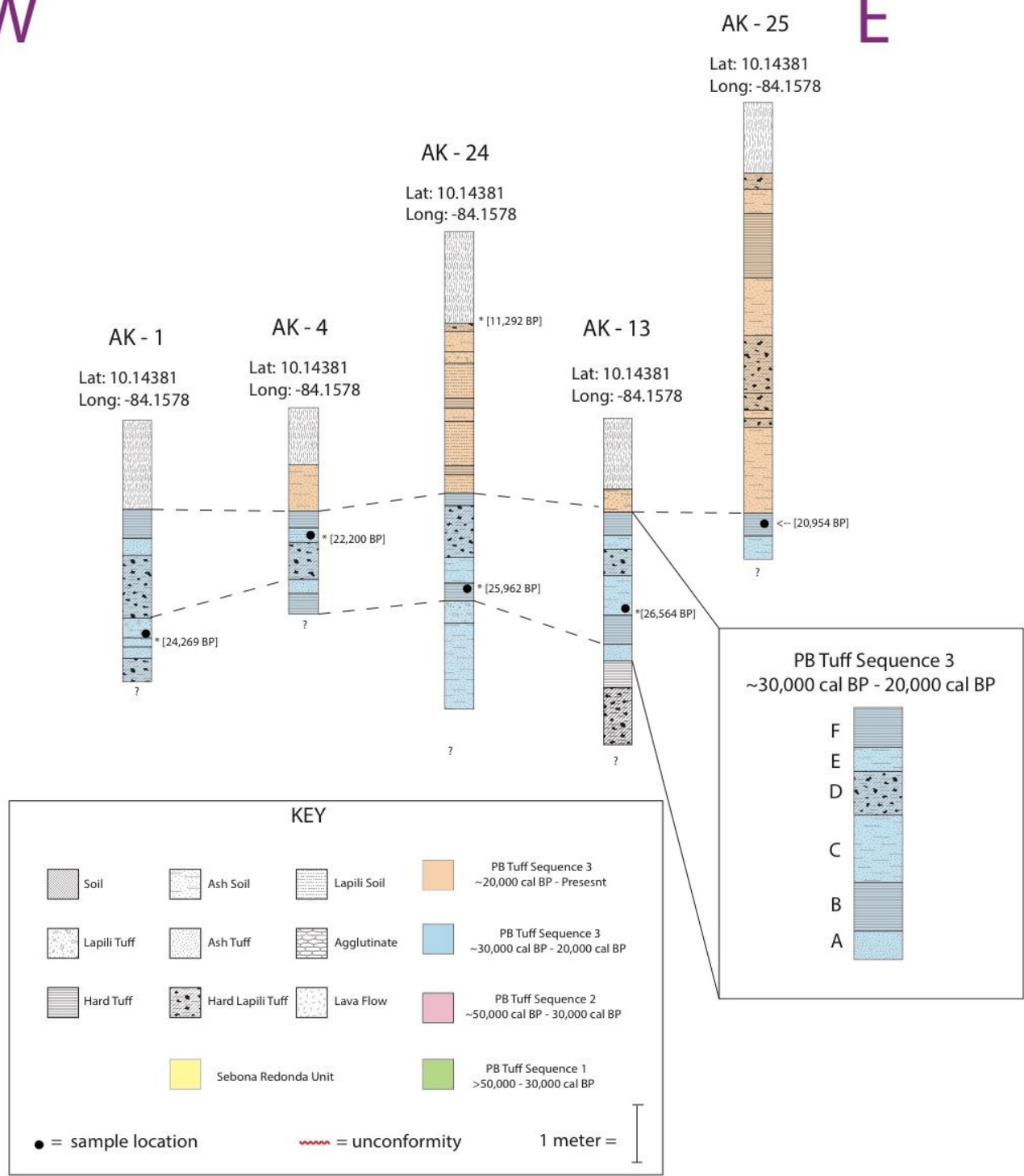


Figure 17: PB Sequence 3 Correlation. The above correlation illustrates the distinctive pattern of tephra deposits observed in PB Sequence 2. The strata are described below.

- A. This layer ranges from an orange-brown lapilli to ash soil to a brownish-gray ash. This layer lies above the hard ash tuff found at the top of the PB Sequence 2 and ranges from about 0.5m to 1.5m. The top portion of this layer contains a high pumice concentration; bombs are 25cm to 30cm.
- B. This layer is not seen in columns north of AK-13. This tephra layer is brownish green in color and can often be seen as a fine-course-ash tuff, but can also be seen as a fine lapilli tuff, like that seen in Column AK-11. The ash ranges from 0.3m to 0.5m in thickness and consists of grain sizes ranging from ≤ 3 mm at its coarsest to about ≤ 0.5 mm.
- C. This is a tephra layer found between the hard brown ash tuff below and an overriding hard lapilli tuff in layer D of the sequence. This layer can appear as a transitional brown lapilli to ash soil, ash, or fine-grained lapilli tuff. This layer averages a thickness of 0.5m but can be seen as thick as 1m. The layer was dated twice with an age range of 24,270 cal BP (column AK-1) to 26,600 cal BP (column AK-13) (Figure 18). This stratum is reddish brown in color and there are about five percent ash fragments present throughout. Column AK-30 is the only column that is missing this layer from the PB Sequence 2 (Figure 26).
- D. The strata consists of a hard lapilli tuff with a large abundance of fine-grained to course-grained pumice (≤ 2.52 cm), with no evidence of grading. Lithic inclusions are as large as 3cm x 1.5 cm. This hard tuff averages a thickness of about 0.5m.
- E. The ash soil found in the strata contains pumice (≤ 3 cm) that makes up less than ten percent of the brown to red matrix. This layer can be as thick as a meter or absent all

- together, as illustrated in the columns in the most eastern flank of the East-West correlation (Figure 26). The ashy soil is capped by the overlying gray hard ash tuff. This layer was dated with an age of 22,200 cal BP.
- F. The hard, gray ash tuff in this layer is fine-grained and light gray in color. The tephra layer is very resistant to weathering and contains small ($\leq 1\text{mm}$) silica deposits that resemble plant roots. This hard tuff caps the PB Sequence 2 was dated at 20,950 cal BP and serves as a barrier for the younger period of volcanic activity found in PB Sequence 4.

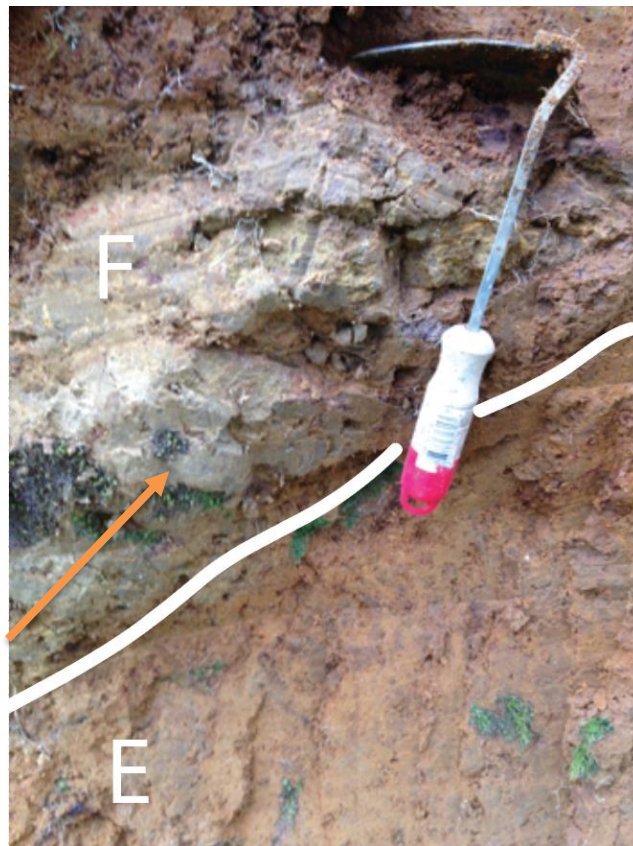


Figure 18: PB sequence 3 (layers E and F). Layers E and F of PB sequence 3 are illustrated in the picture above. Layer F consists of a hard gray ash tuff and below is the ashy soil layer. The white veins are indicated by the orange arrow.

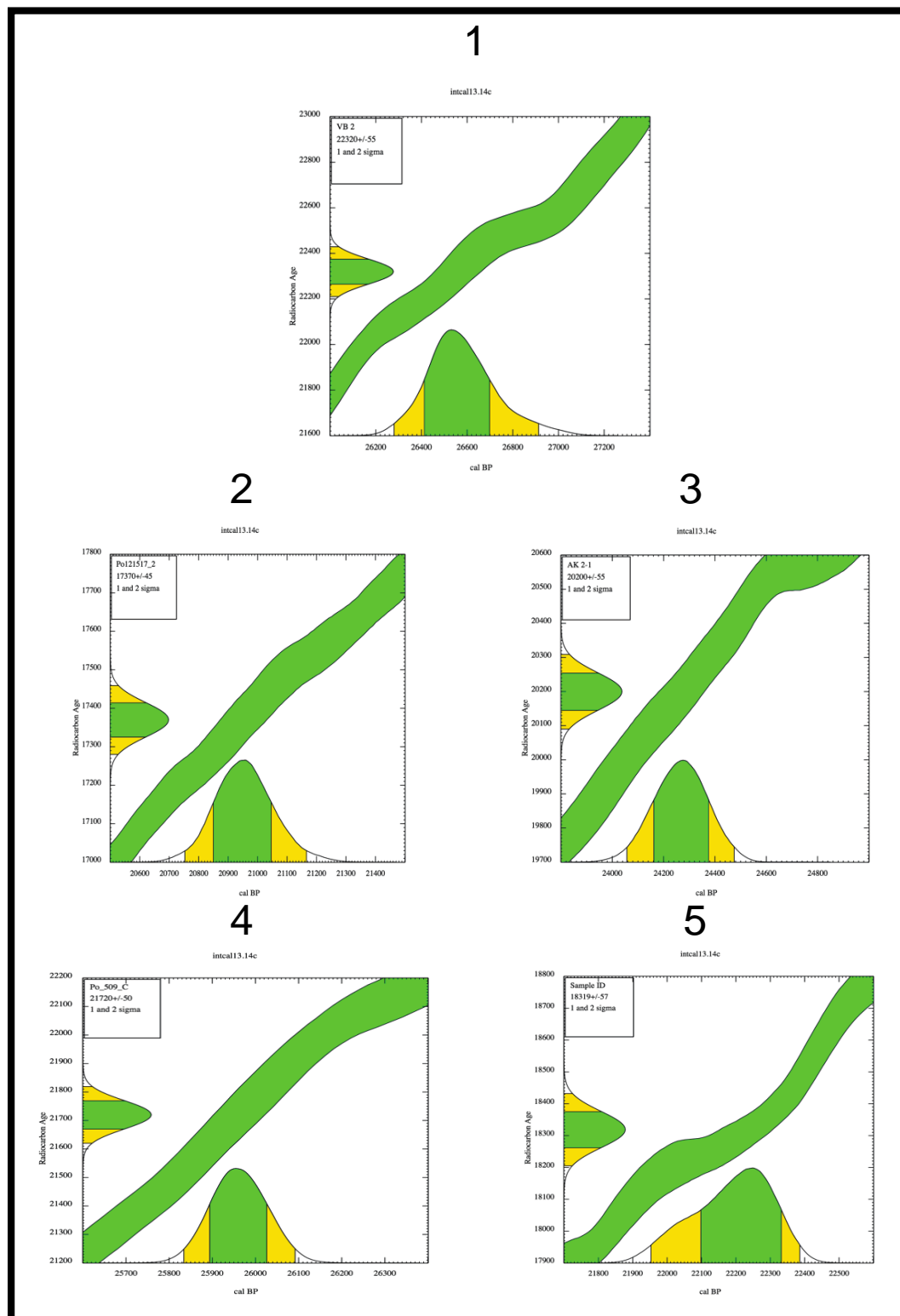


Figure 19: Calibration curves of PB Sequence 3. The calibration curves above were created with the Calib calibration software. Graph 1 coincides with layer F, graph 2 coincides with layer E,

graphs 3 and 4 resulted from the samples in layer C, and graph 5 is the calibration associated with sample taken from layer B.

4.3.5 *PB Sequence 4*

The most recent tephra layers are found in the fourth PB Tuff Sequence. The representation of this sequence contains the greatest amount of variance between stratigraphic columns (Figures 24-27). The bottom portion of this tuff sequence is defined by a fine ash soil that was dated at 17,320 cal BP. This sequence has a thicker and more complete history toward the east, closer to the Botos crater. One of the most recent eruptions dates to 1953-1955 AD, in which the eruptions were classified as phreatomagmatic, strombolian and pyroclastic surges. The pyroclastic surges resulted in a defined white ash layer found in column AK-26.



Figure 20: PB Sequence 3 outcrop modern eruptions. The white ash layer represents layer E in PB sequence 4, as depicted in Figure 18.

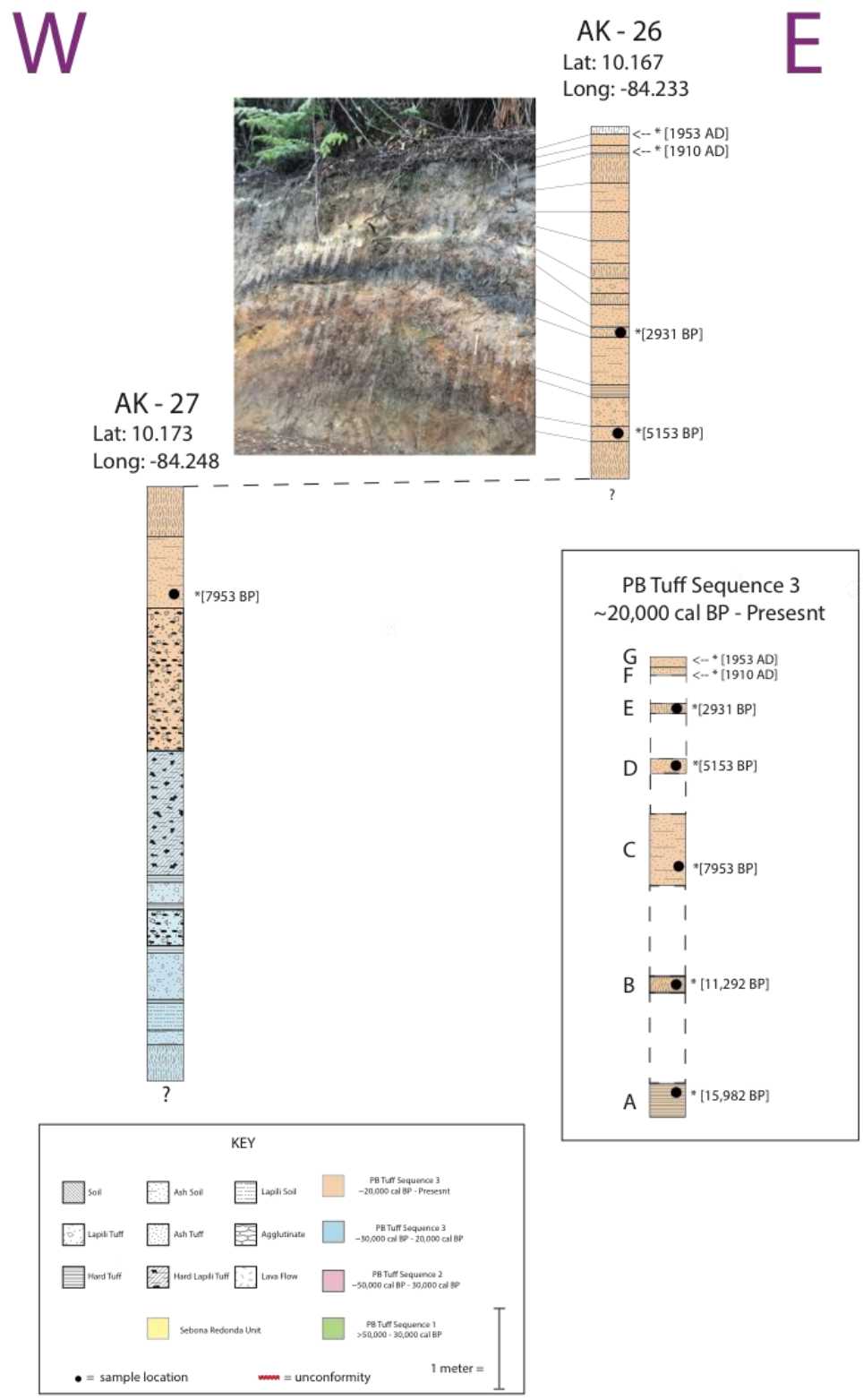


Figure 22. PB Sequence 4 Correlations B. The correlations from Figure (22) were used to create the Figure above of PB Sequence 4. The tephras within PB Sequence 4 are highly variable, so the volcanic sequence was summarized by omitting layers found between the dated tuffs.

4.4 Further Implications

The columns were placed into two series of correlations, one running north-south and one running east-west (Figure 1). The correlations were broken into four sectors (Figures 24-27). The western and northern sectors contain columns located on the eastern slope of the Poás volcano, while the eastern and southern sectors contain columns that encompass the valley between Barva and Poas that lies northwest of the Barva volcano Crater (Figure 1).

N

S

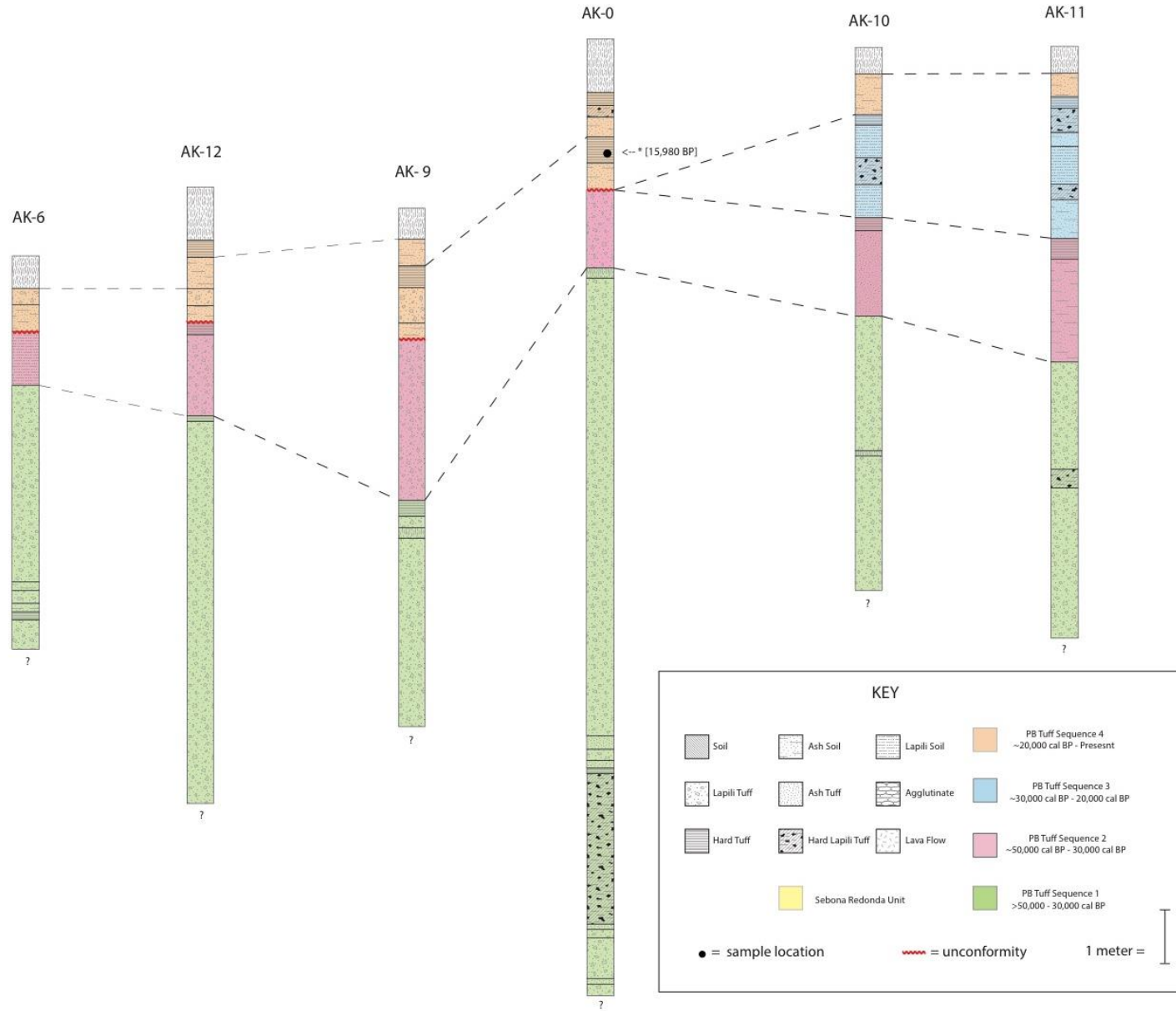


Figure 23: North-South-Sector A. Correlation for the northern most portion of the north-south correlation that lies between the Barva and Poás volcanoes. In this correlation, the PB Sequence 1, 2, and 4 are present in all of the columns. PB sequence 3 is only found in AK-10 and AK-11, which has been interpreted as an unconformity because the AK-0 and AK 10 are only one kilometer of each other. This correlation only contains one C^{14} age, found in column AK-0, due to the lack of organic material present within the surrounding columns.

N

S

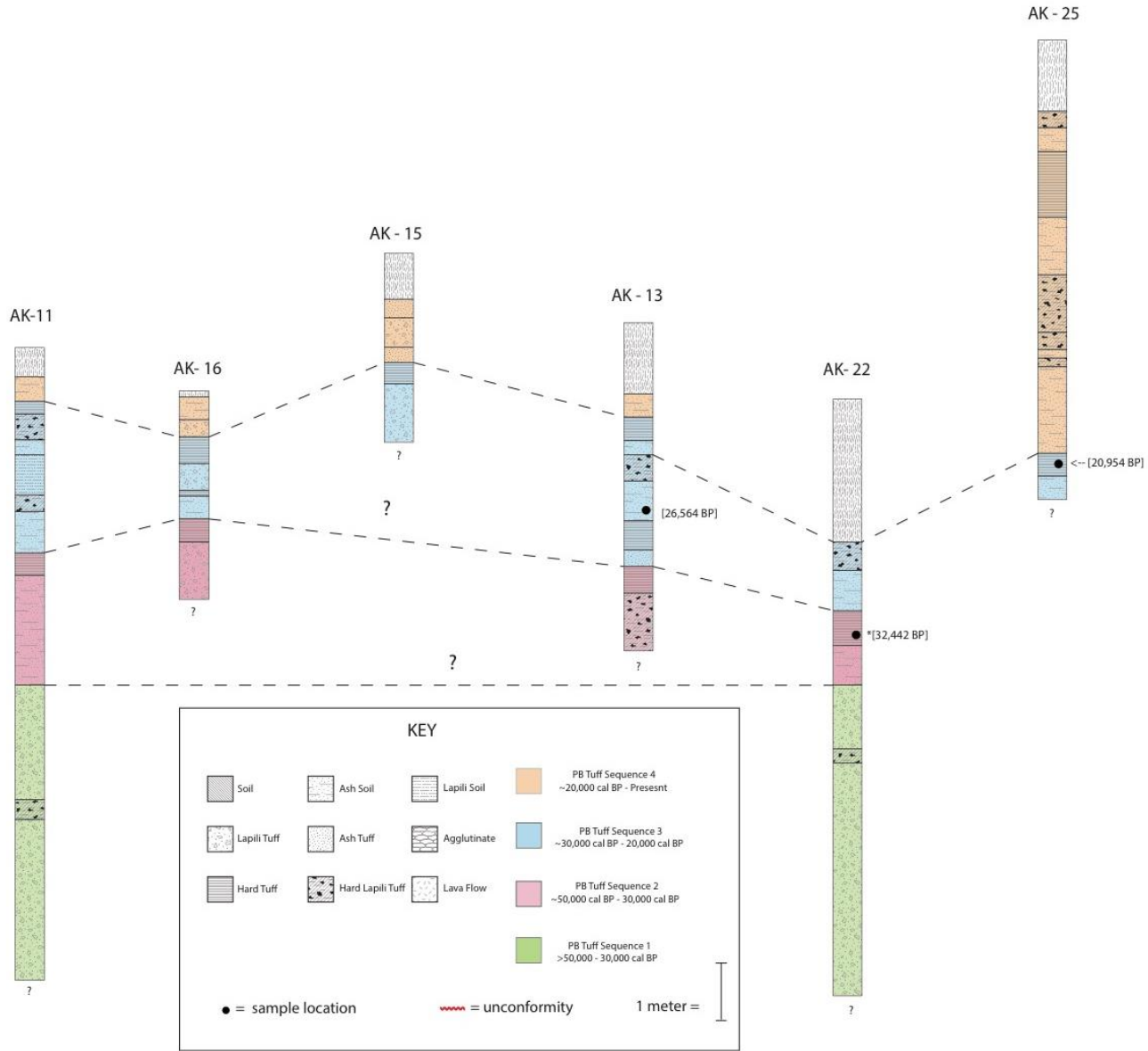
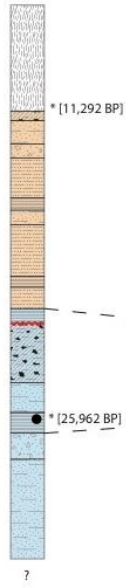


Figure 24: North-South-Sector B. Correlation for the southernmost portion of the north-south correlation that lies between Barva and Poás volcanoes. The correlation incorporates three carbon-14 ages. Layer A of PB Sequence 2 is found as more course-grained in column AK-13. AK-25 has the thickest PB Sequence 4 in the correlation above.

W

E

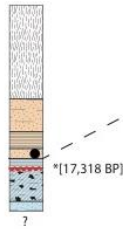
AK - 24



AK-30



AK - 29



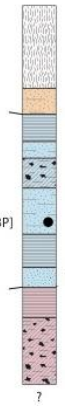
AK-11



AK-16



AK - 13



AK - 0

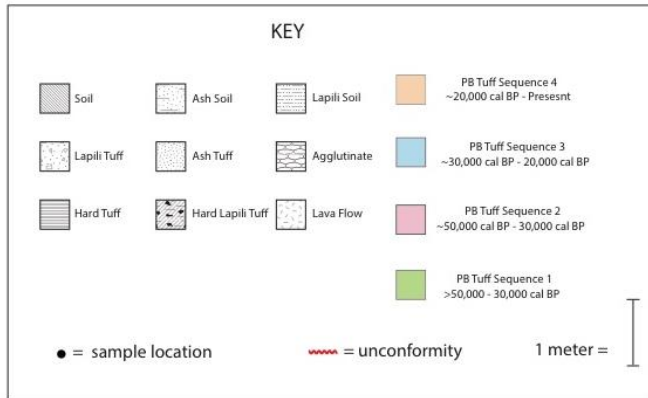


Figure 25: East-West-Sector C. Correlation for the eastern most portion of the east-west correlation that lies between Barva and Poás. The correlation of AK 0 is problematic, as it does not contain layer B of PB Sequence 2 and is missing PB Sequence 3. This is interpreted as an unconformity. Another unconformity is found in columns AK-24, AK-30, AK-29, and AK-11 between layers D and F in PB sequence 3.

W

E

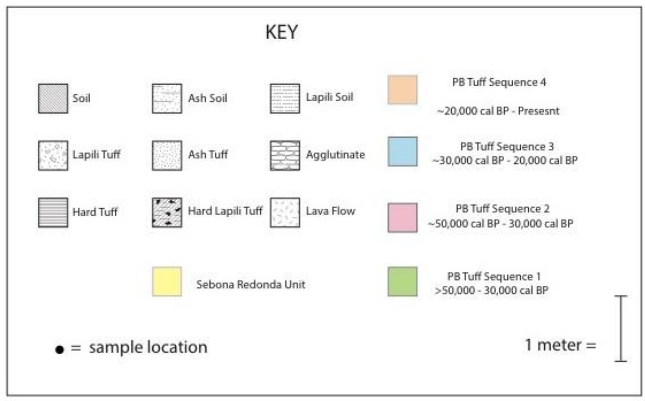
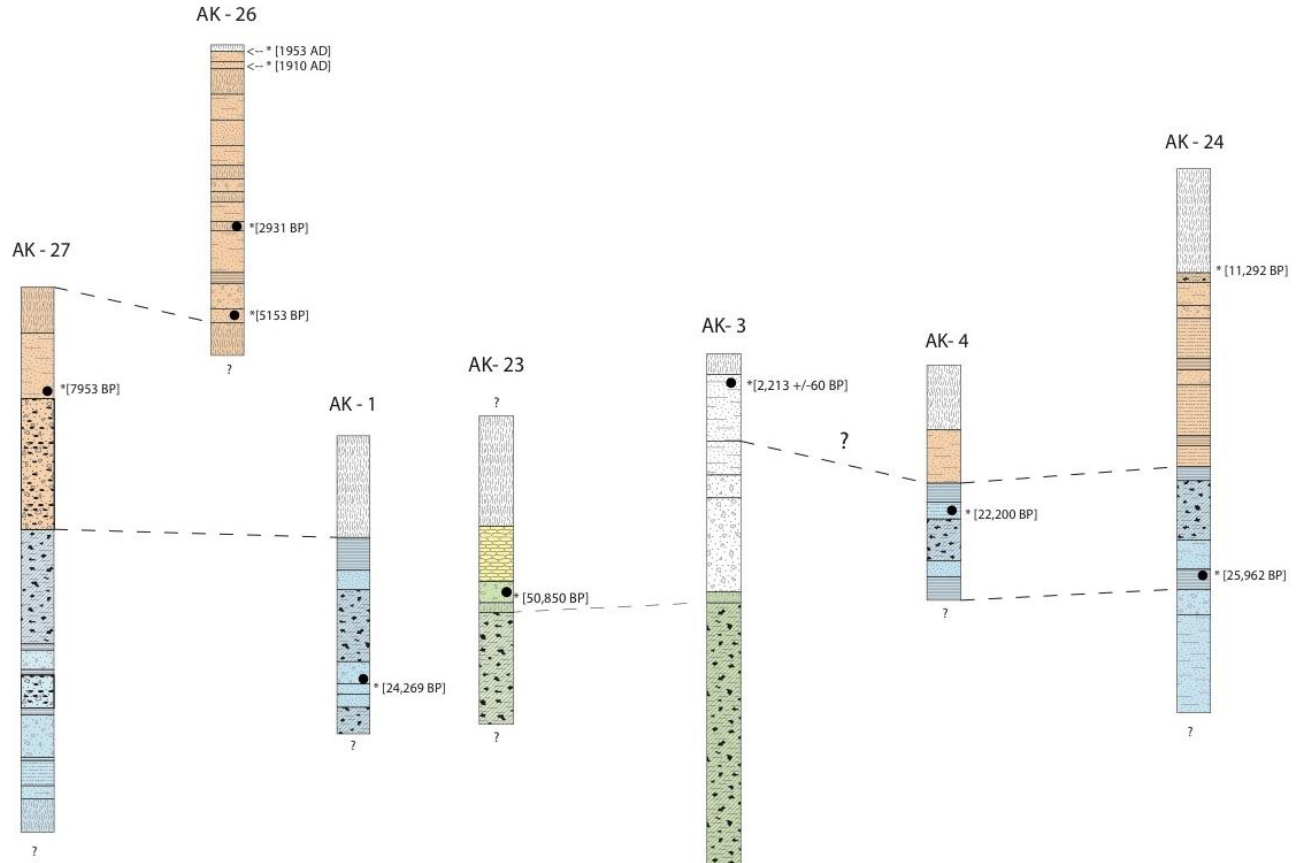


Figure 26. East-West Sector D. Correlation for the western most portion of the east-west correlation that lies between Barva and Poás. The exact correlation of column AK-1 to AK23 is not well known. The representation from 50,000 BP to the present is represented by the correlation above. It is expected that PB sequence 2 and 3 lie within column AK-3, but because of the uncertainty of the correlation, it was not indicated.

4.4.1 Northern Sector A

The correlations for the northern portion of the north-south series of stratigraphic columns is called the northern flank. This correlation portion incorporates the least amount of carbon-14 dates, 15,982 cal BP (see table 1 and Figure 24), including only one from column AK-0, dated at 15,980 cal BP. The tephra deposits found in the northern portion of the map are different from those found in any other series of correlations in the study area, as the columns have very thick (4-9m) lapilli layers and do not have the distinguishable hard tuff layers by which to correlate them (see Figure 24). The lapilli layers found in the northern portion of the map also lack organic material, limiting sample collection for this area. The lapilli tuffs in the northern sector less resistant to weathering and contain less hard tuff layers. The presence of hard tuff in the upper portion of columns AK-10 and AK-11 were identified with sections of PB Tuff Sequence 3, but the tuff sequence could not be identified north of column AK-10. This was an implication that either the layers had pinched out from the source, or there was an unconformity present. Altogether, this series of correlations is less reliable due to the lack of available carbon-14 ages.

4.4.2 Southern Sector B

The correlations for the southern portion of the north-south series of correlations is called the southern flank. There are three ages, located in the most southern columns, included in this correlation. PB Sequence 1 and 2 are relatively consistent throughout the columns in this sector, because the lapilli tuffs in PB Sequence 1 are 4-5m thick, separated by a hard tuff, and PB Sequence 2 has a hard ash tuff layer of about 0.5m throughout (see Figure 25). The ages on the right in Figure 25 assure more accurate correlations between hard ash tuff layers. PB Sequence 4

has a larger exposure in column AK-25 than in any other column in this correlation series, implying that the PB Sequence 4 deposits in AK-25 may be traced to Barva. The 4km distance that lies between AK-25 and the closest column, AK-22, could be an explanation for the lack of exposure of the PB Sequence deposits seen in column AK-25 (see Figure 25). Deeply weathered deposits in column AK-22, indicated by the large layer of topsoil, could explain the lack of exposure of PB Tuff Sequence 4 in the column (see Figure 25). AK-14 and AK-15 are relatively shallow columns and therefore are correlated by the hard ash tuff at the top of PB Tuff Sequence 3.

4.4.3 Eastern Sector C

The correlations for the eastern portion of the east-west series of correlations is called the eastern sector (Figure 26). Five carbon-14 samples were incorporated in this section, 11, 292 cal BP, 15,982 cal BP, 17,318 cal BP, 25,962 cal BP, and 26, 564 cal BP (refer to table 1 and Figure 27), and PB 1 through 4 Sequences were identified. The diagnostics pattern in PB Sequence 3 (Figure 28) permitted many of the correlations within the western sector (Figure 27). The top and bottom units of PB Sequence 3 are present in all of the columns, with the exception of AK-0, in the eastern sector, creating clear distinctions between volcanic periods and more apparent correlations. Layer E from PB Sequence 3 is absent from many of the columns, which may be due to an unconformity between Layer D of PB Sequence 3. The correlation of column AK-0 is only possible by distinguishing the periods of volcanic activity, because focusing on the correlation of the individual tuff layers is problematic here, due to the lack of hard tuffs that have aided in other correlations. AK-0 is located 3km north of AK-13, which can account for some of the missing tephra units, as layers pinch out as they move from the source. The two columns (AK-13 and AK-0) have tephra facies that are drastically different. AK-0 three thin (<0.5m) hard

tuffs underlain by large lapilli tuffs (as large as 9m), while AK-13 contains multiple hard ash and lapilli tuffs throughout that appear as thick as 1m. The only connection to correlation AK-0 and AK-13 was by identifying and correlating their exposures of PB tuff sequence 2. The collection of more columns in the areas between AK-0 and AK-13 that contain organics would be beneficial and could improve this correlation. The bottom hard ash tuff in the top portion of column AK-0 has a date of 15,982 cal BP, which placing this layer and those that overlay it in a period of volcanic activity less than 20,000 BP (PB Tuff Sequence 1). The absence of all of the PB Tuff Sequence 3 layers has led to my hypothesis of a large unconformity.

4.4.4 Western Sector D

The correlations for the western portion of the east-west flank of correlations is called the Western Sector, illustrated in Figure 27. This correlation is inherently the most reliable of the correlation sectors because contains eleven ages that range from 50,850 BP to 1953 AD, nine of which are carbon-radiometric ages collected and dated in this study. Two of the ages were inferred from layer descriptions made by (Campaña Geológica, 2004). AK-26 and AK-27 are the two columns found furthest west, and columns lie within 2.5km of the Poás crater (Figure 1). These columns contain the most recent deposits from Poás. Their proximity to emission centers result is a thicker PB Sequence 4, and many thin layers disappear with increasing distance from the crater as they represent minor events (Figure 27). The next column in this sector is AK-1, which does not include any of the PB Sequence 4 units. The column does, however, have a thick topsoil in which some of the tuffs from PB sequence 4 could be camouflaged due to heavy oxidation. The correlation between AK-1 and AK-3 is challenging because AK-3 lacks the diagnostic PB Sequence 3 pattern (Figure 28), making PB Sequence 2 and 4 difficult to identify.

AK-3 has a height of about 8 meters with tephrastatigraphic representation from 50,850 BP to 2,213 cal BP. The height of the column is relatively low for the expansive time range. AK-3 is located within a kilometer of AK-1, so the drastic change in tephra deposits found between the columns can be inferred as very low sedimentation rates (i.e. halted volcanic activity), presence of unconformities, or a combination of the two. AK-23 was easily correlated, by visually tracing the Sabana Redonda unit (agglutinate layer) along the road. as it is located only 40m west of column AK-3. Ak-3 and Ak-4 were correlated by inferring that the hard tuff found in column AK-3 was that of layer D in PB Sequence 3 (Figure 18). The AK-4 correlation to column AK-24 is easily made using the characteristic pattern and dated hard ash tuff B of PB Sequence 3 (Figure 28).

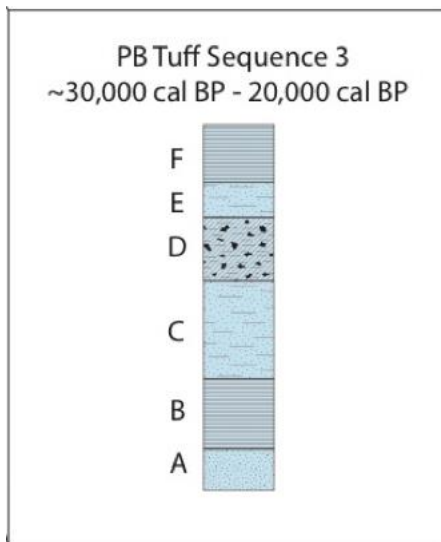


Figure 27: Diagnostic of PB Sequence 3. Diagnostic pattern observed in PB sequence 3. Layer descriptions are described in pages 39 and 40.

4.4.5

4.4.6

4.5 Spatial Relationships

When the correlations are placed side by side to create one complete run of east-west correlations, and one complete run of north-south correlations, certain spatial relationships are visually identifiable. PB Tuff Sequence 3 begins to thin as it migrates to the eastern portion of the correlation (see Figures 26 and 27). The tuff sequence also tapers to the north, as it is not seen in columns north of AK-10, due to either thinning units or an unconformity within AK-0. The deposits of layer A of PB Tuff Sequence 2 thickens to the north, while layer B of the sequence begins to taper, although this could be attributed to an unconformity, because the erosional contact falls at the interface of layer B of PB Tuff Sequence 4 and PB sequence 4 (see Figure 22). PB Tuff Sequence 4 varies in thickness throughout the columns, but appears to thin in the center of the valley and thicken towards the both Poás and Barva volcanoes. The tuffs of found in sequence 4 increase in grain size as they approach the Poás crater to the west and the Barva crater to the east. Many of the tephra layers decrease in thickness to the north, which can be attributed to prevailing winds originating from the northeast and flowing towards the southwest.

4.5.1 Barva

PB Tuff Sequence 1 is comprised of thick poorly sorted lapilli tuffs that underlay much of the strata within the study area. Because of the stratigraphic position of this sequence, the large lapilli tuffs are dated to be much older than 50,000 BP. Barva has been characterized as the source of large pyroclastic eruptions with large volumes of fall and pyroclastic flow deposits(

Stine, 1991). The chronostratigraphic record for Barva has tephra intermixed with thick (1-2m) soils (Arredondo & Soto, 2006). The large lapilli tuffs that make up PB Sequence 1 are likely associated with plinian eruptions from the Barva crater.

4.5.2 Poás

Past volcanic activity from Poás has been characterized by phreatic and phreatomagmatic eruptions from the caldera that formed over 40,000 years ago (Walker, 1982). These types of eruptions result in poorly sorted tephra layers with scoria inclusions, such as those found in layer D of PB Tuff Sequence 3. The Poás crater is oriented along the same fracture network that the Sabana Redonda Unit is found. The fracture cultivated magmatic interaction with groundwater, resulting in cones of scoria that originated from phreatomagmatic eruptions. Today, Poás experiences infrequent phreatic and strombolian eruptions of mud, ash and pumice deposits that can travel up to 12km from the crater (Walker, 1982).

5 CONCLUSIONS

The complexity of the highlands of the Cordillera Central can be attributed to overlapping deposits from various volcanic centers, a highly erosive tropical environment, and a range of unconformities present, which make unraveling the eruptive history of the area between the Barva and Poás volcanoes problematic. The complexity of the area was overcome by making correlations between stratigraphic columns, supported by fourteen stratigraphically constrained C^{14} ages, generated in this study to produce one composite column. The construction of the composite column was contingent upon the correlations made in the north-south and east-west correlation sequences. The average thickness of each layer in each tuff sequence (PB Sequence 1, 2, 3, and 4) was calculated and used in the composite column. The type of tuff illustrated for

each tephra layer in the composite column was determined by observing the deposit that occurred most frequently within each layer.

Relying on correlations based on physical characteristics alone lends itself to inaccuracy due to levels of variance in tephtras throughout the study area. The stratigraphic correlations made in Figures 24-27 served as the foundation for creating the composite column illustrated in Figure 29. The largest plinian eruption, was found below the agglutinate layer dated at 50,000 years ago, and it was determined that that plinian event was likely linked to Barva. Through observation and analysis of the tephra stratigraphy present, it is also determined that there has not been a large plinian eruption from either the Barva or Poás volcano in the last 30,000 years.

Much of the recent volcanic deposition in the study area can be attributed to that produced by the main crater of Poás, with a sedimentation rate of about one meter of sediment for every one thousand years. The volume of ejecta with each event has experienced a noticeable decrease over the past 50,000 years, particularly in the last 5,000 years. Although the number of pulses have appeared to increase, the intensity and extent has diminished. The tephra-stratigraphy from the last 7,000 years is believed to have been a result of volcanic activity from Poás, due to the proximal extent and thickness ($\leq 60\text{cm}$) of the layers from the crater.

The inherent dangers associated with Alajuela, are primarily linked to Poás due to its recent activity, but have been found to be relatively low. Although the hazards of Poás are reasonably low for people living near the National Park, businesses based in crops and livestock are still at risk of being affected by ash plumes carried downwind. For surrounding establishments that thrive on the business brought in by tourists, the potential for future eruptions plays a huge role on their livelihood.

Now, there is a complete chronostratigraphy of the area, and correlations made for both the Barva Formation (Arredondo & Soto, 2007) and the Poás members (Sanchez-Murillo, 2016) can be updated in an effort to create more reliable hazard maps. The hazard maps created would be invaluable to the population that surround these two volcanoes.

Composite Column

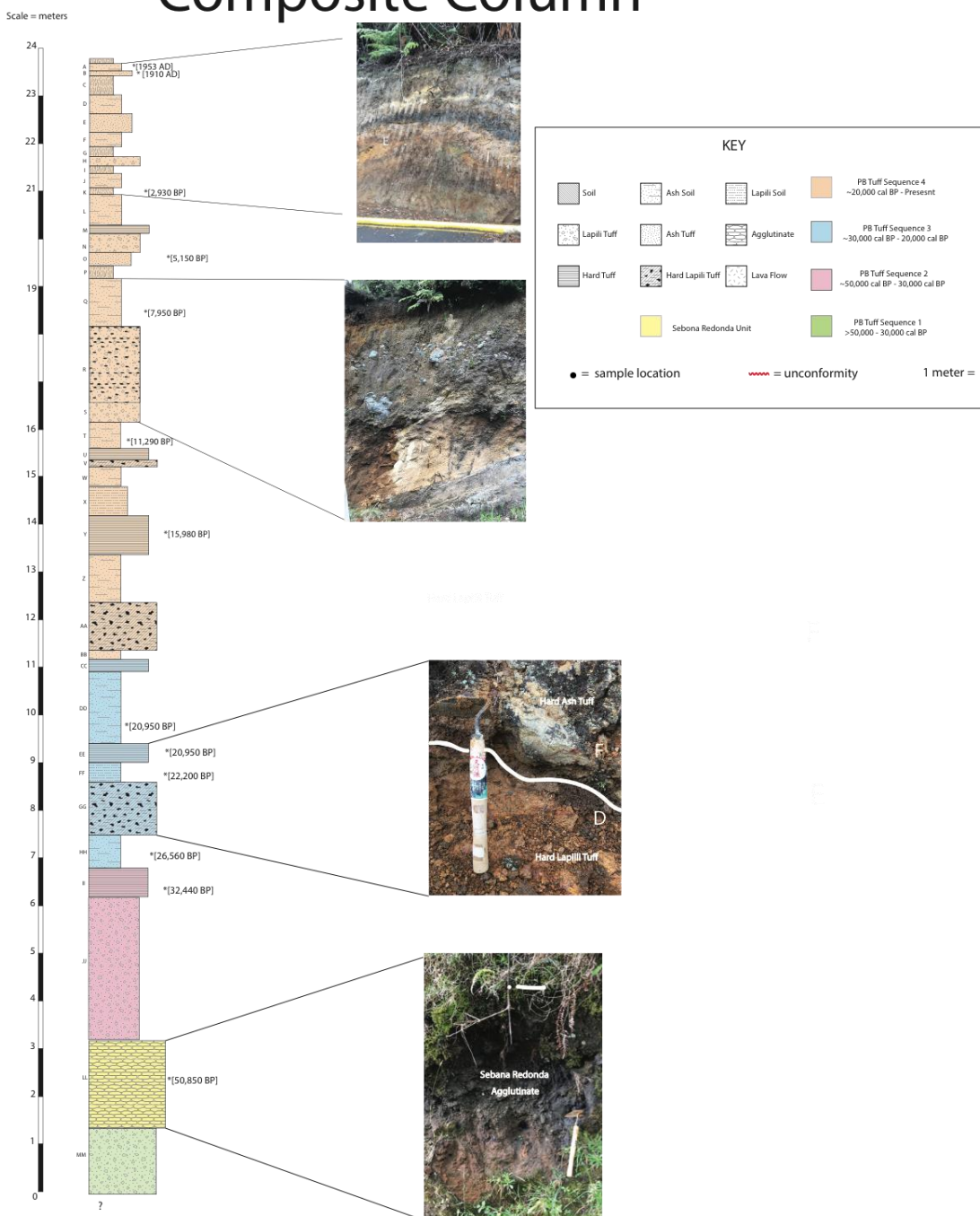


Figure 28: Composite Column. The composite column above was constructed using the correlations in figures 23-25. This represents the complete eruptive history of the fall deposits that have accumulated in the study area from the last 50,000 years.

6 RECOMMENDATIONS

Using the dates from this study to make improvements upon past correlations is imperative for future studies, as improper correlations can lead to incorrect interpretations for isopachs and isopleths. More stratigraphic columns should be made in locations that lie in the northern sector of the map, concentrating on the southern of Barva. Careful measurements of grain sizes should be taken to ensure precision on isopach and isopleth interpretations in order to accurately assess the eruptive nature of this area to create hazard maps. Using the carbon-14 dates and layer descriptions, future work could correlate tephra layers to new columns, especially with new carbon-14 sample collections. The hazard map produced in a future study using this method would serve as a replacement for older maps that have been produced without the certainty instilled by carbon-14 dating. The lives and livelihood of thousands would depend upon the accuracy of this map.

REFERENCES

- Branney, M., & Acocella, V. (2015). Chapter 16 - Calderas A2 - Sigurdsson, Haraldur. In *The Encyclopedia of Volcanoes (Second Edition)* (pp. 299–315). Amsterdam: Academic Press.
<https://doi.org/10.1016/B978-0-12-385938-9.00016-X>
- CAMPAÑA GEOLÓGICA, 2004: Estudio geológico en el cantón de Poás, provincia de Alajuela.- 168 págs. Univ. de Costa Rica, San José [Inf. Campaña Geol.]
- Cioni, R., Pistolesi, M., & Rosi, M. (2015). Chapter 29 - Plinian and Subplinian Eruptions A2 - Sigurdsson, Haraldur. In *The Encyclopedia of Volcanoes (Second Edition)* (pp. 519–535). Amsterdam: Academic Press. <https://doi.org/10.1016/B978-0-12-385938-9.00029-8>
- Deligne, N. I., & Sigurdsson, H. (2015). Chapter 14 - Global Rates of Volcanism and Volcanic Episodes. In *The Encyclopedia of Volcanoes (Second Edition)* (pp. 265–272). Amsterdam: Academic Press. <https://doi.org/10.1016/B978-0-12-385938-9.00014-6>
- De Moor, J. M., Aiuppa, A., Pacheco, J., Avard, G., Kern, C., Liuzzo, M., ... Fischer, T. P. (2016). Short-period volcanic gas precursors to phreatic eruptions: Insights from Poás Volcano, Costa Rica. *Earth and Planetary Science Letters*, 442, 218–227.
<https://doi.org/10.1016/j.epsl.2016.02.056>
- de Silva, S., & Lindsay, J. M. (2015). Chapter 15 - Primary Volcanic Landforms A2 - Sigurdsson, Haraldur. In *The Encyclopedia of Volcanoes (Second Edition)* (pp. 273–297). Amsterdam: Academic Press. <https://doi.org/10.1016/B978-0-12-385938-9.00015-8>
- Fischer, T. P., Ramírez, C., Mora-Amador, R. A., Hilton, D. R., Barnes, J. D., Sharp, Z. D., ... Shaw, A. M. (2015). Temporal variations in fumarole gas chemistry at Poás volcano, Costa Rica. *Journal of Volcanology and Geothermal Research*, 294, 56–70.
<https://doi.org/10.1016/j.jvolgeores.2015.02.002>

- GAZEL, E. & RUIZ, P., 2005: Los conos piroclásticos de Sabana Redonda: componente magmático enriquecido del volcán Poás, Costa Rica.- *Rev. Geol. Amér. Central*, 33: 45-60.
- Horn, S. P. (2013). The age of the Laguna Hule explosion crater, Costa Rica, and the timing of subsequent tephra eruptions: evidence from lake sediments. *Revista Geológica de América Central* /, (24).
- Houghton, B., & Carey, R. J. (2015). Chapter 34 - Pyroclastic Fall Deposits A2 - Sigurdsson, Haraldur. In *The Encyclopedia of Volcanoes (Second Edition)* (pp. 599–616). Amsterdam: Academic Press. Retrieved from <https://www.sciencedirect.com/science/article/pii/B9780123859389000341>
- Martínez, M., Fernández, E., Valdés, J., Barboza, V., Van der Laat, R., Duarte, E., ... Marino, T. (2000). Chemical evolution and volcanic activity of the active crater lake of Poás volcano, Costa Rica, 1993–1997. *Journal of Volcanology and Geothermal Research*, 97(1–4), 127–141. [https://doi.org/10.1016/S0377-0273\(99\)00165-1](https://doi.org/10.1016/S0377-0273(99)00165-1)
- PROSSER, J.T., 1983: The geology of Poás volcano, Costa Rica.- 165 pags. Darmouth Collegue, New Hampshire [Tesis MSc.]
- Prosser, J. T., & Carr, M. J. (1987). Poás volcano, Costa Rica: Geology of the summit region and spatial and temporal variations among the most recent lavas. *Journal of Volcanology and Geothermal Research*, 33(1–3), 131–146. [https://doi.org/10.1016/0377-0273\(87\)90057-6](https://doi.org/10.1016/0377-0273(87)90057-6)
- Pyle, D. M. (2015). Chapter 13 - Sizes of Volcanic Eruptions A2 - Sigurdsson, Haraldur. In *The Encyclopedia of Volcanoes (Second Edition)* (pp. 257–264). Amsterdam: Academic Press. https://doi.org/10.1016/B978-0-12-385938-9.00013-4costa_rica_volcano_profile.pdf. (n.d.).
- Rodríguez, A., Eggenkamp, H. G. M., Martínez-Cruz, M., & van Bergen, M. J. (2016). Chlorine isotope and Cl–Br fractionation in fluids of Poás volcano (Costa Rica): Insight into an active

volcanic–hydrothermal system. *Journal of Volcanology and Geothermal Research*, 325, 70–85. <https://doi.org/10.1016/j.jvolgeores.2016.05.020>

Rodríguez, A., & van Bergen, M. J. (n.d.). Superficial alteration mineralogy in active volcanic systems: An example of Poás volcano, Costa Rica. *Journal of Volcanology and Geothermal Research*. <https://doi.org/10.1016/j.jvolgeores.2017.04.006>

Rowe Jr., G. L., Brantley, S. L., Fernandez, J. F., & Borgia, A. (1995). The chemical and hydrologic structure of Poa's Volcano, Costa Rica. *Journal of Volcanology and Geothermal Research*, 64(3–4), 233–267. [https://doi.org/10.1016/0377-0273\(94\)00079-V](https://doi.org/10.1016/0377-0273(94)00079-V)

Sadler PM (1999) The influence of hiatuses on sediment accumulation rates. *GeoRes Forum* 5:15–40. http://tectonics.caltech.edu/meetings/journal_club/session1/Sadler1999TransTech.pdf

Siebert, L., Cottrell, E., Venzke, E., & Andrews, B. (2015). Chapter 12 - Earth's Volcanoes and Their Eruptions: An Overview A2 - Sigurdsson, Haraldur. In *The Encyclopedia of Volcanoes (Second Edition)* (pp. 239–255). Amsterdam: Academic Press. <https://doi.org/10.1016/B978-0-12-385938-9.00012-2>

Stine CM, Banks NG (1991) Costa Rica volcano profile. USGS open file report 91-591.

Vallance, J. W., & Iverson, R. M. (2015). Chapter 37 - Lahars and Their Deposits A2 - Sigurdsson, Haraldur. In *The Encyclopedia of Volcanoes (Second Edition)* (pp. 649–664). Amsterdam: Academic Press. <https://doi.org/10.1016/B978-0-12-385938-9.00037-7>

Walker, J.P.L., 1982, Volcanic Hazard: *Boletín de Vulcanología*, v. 14, p. 41-48.

APPENDICES

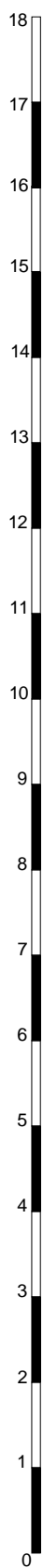
AK-0



* [15,980 +/- 92 BP]

AK- 1

Scale = meters



Lat: 10.156
Long: -84.22



AK-3

Scale = meters

Lat: 10.155
Long: -84.214



AK-13

Scale = meters

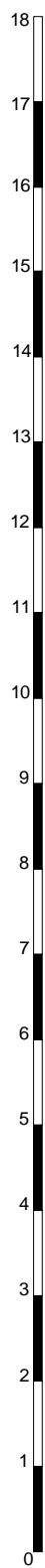
Lat: 10.152
Long: -84.149



AK-24

Scale = meters

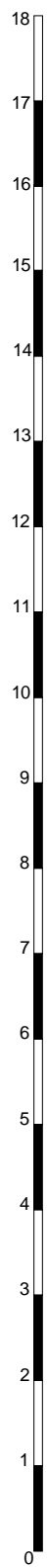
Lat: 10.157
Long: -84.193



1.0000

AK-22

Scale = meters



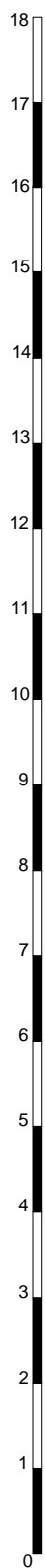
Lat: 10.143
Long: -84.157

0.000000
0.000000
0.000000

AK - 25

Scale = meters

Lat: 10.139
Long: -84.161



1.0000

AK-26

Scale = meters



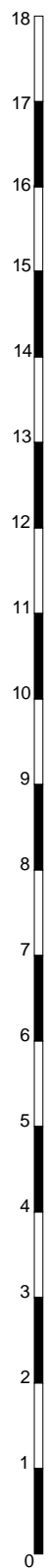
Lat: 10.167
Long: -84.233

24

AK-27

Scale = meters

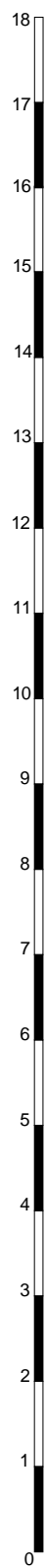
Lat: 10.173
Long: -84.248



1.

AK - 29

Scale = meters



Lat: 10.163
Long: -84.193

1.